A critical review of bioceramics for magnetic hyperthermia

Bioceramics for Magnetic Hyperthermia

Omid Sedighi[1 $], Amirhossein Alaghmandfard[1 $], Maziar Montazerian[2,*], Francesco Baino[3,#*], ...

1- Department of Materials Science and Engineering, Sharif University of Technology, Tehran, Iran

2- ...

3- Institute of Materials Physics and Engineering, Department of Applied Science and Technology, Politecnico di Torino, Torino, Italy

$: Authors contributed equally to this work.

#: Member of the American Ceramic Society.

* Corresponding authors: MM (maziar_montaz@yahoo.com) & FB (francesco.baino@polito.it)

Abstract

Magnetic hyperthermia (HT) using biocompatible ceramics is a ground-breaking, competent, and safe thermo-therapeutic strategy for cancer treatment. The magnetic properties of bioceramics, along with their structure and synthesis parameters, are responsible for controlled heating of malignant tumors and are the key to clinical success. After providing a brief overview of magnetism and its significance in biomedicine, this review deals with materials selection and synthesis methods of bioceramics/glasses used for HT. Relevant researches carried out on promising bioceramics for magnetic HT, with focus on their size, shape, surface functionalization, magnetic field parameters, and in vitro/vivo properties to optimize cancer therapy, are also discussed. Recent progress in magnetic HT combined with chemotherapy, radiotherapy, and phototherapy is especially highlighted, with the aim to provide interdisciplinary knowledge to advance further the applications of bioceramics in this field.

Keywords: Bioceramic; Glass; Nanomaterials**;** Cancer; Hyperthermia

1- Introduction

Hyperthermia (HT) is a rapid cancer therapy inducing cellular apoptosis by increasing the local temperature of cancerous tissues between 41 ^{o}C and 43 ^{o}C. The tumors are highly susceptible to this thermal range at which cancerous cells are destroyed, while the normal cells undergo no significant damaging effects. HT is induced by using magnetic materials under an alternating magnetic field (AMF). Benefitting from some favorable characteristics of magnetic nanomaterials (MNPs), magnetic HT has drawn enormous attention and reduced the adverse side effects related to conventional treatments of several tumors such as prostate, glioblastoma, metastatic bone cancer, etc. This method is usually combined with other therapeutic approaches like chemotherapy (drug delivery), radiotherapy, photothermal therapy, gene therapy, immunotherapy, and high intensity focused ultrasound, which are critically discussed in this paper [1].

Both biocompatible ceramics and glasses are considered for different HT biomedical applications [2 -5]. Several bioceramics could be mainly used as thermo-seeds for HT cancer treatment. Particularly, nanostructured bioceramics are primarily employed under alternating magnetic field (AMF) to provide adequate heat and local temperature increase up to 43 ^{o}C. Besides, biocompatible glass-ceramics (GCs) are also widely investigated for this application. Iron oxide-based nanomaterials, including magnetite and maghemite nanoparticles, have captured considerable attention, and this is due to their relatively easy preparation approach, being controllable, having low cytotoxicity, and overall tunable properties. In addition to oxide-based MNPs used for this application, other metallic materials like nickel, cobalt, etc., are intensively used to improve heating efficiency and treatment feasibility. In order to enhance heat generation efficacy, reducing the particle size and lowering the Curie temperature are two indispensable approaches [5].

Several kinds of clinical researches have been reported on this therapeutic approach since 2006. The first clinical study done on the magnetic HT was employed to treat glioblastoma multiform. This research was performed on 14 patients, who all received an average of 6-time treatments following about 0.2 ml magnetic fluid per ml tumor volume and the single fraction of 2 Gy of radiotherapy of average 30 Gy. It was demonstrated that using aminosilane-coated iron

oxide nanoparticles (IONPs) for magnetic HT provided a temperature of about 44.6 ^{o}C. It was also revealed that magnetic HT was a safe treatment for glioblastoma multiform [4]. In another research, a magnetic fluid including IONPs dispersed in water was employed for magnetic HT, and the results revealed that magnetic thermotherapy could be well-designed in the treatment of solid tumors [5]. In this work, Wust et al. concluded that the moderate H-field increase leads to enhancing the coverage, promoting the nanofluid-based heating technology's therapeutic efficiency. To be more specific, the 2 kA/m increase in the H-field results in the improvement of 42 ^{o}C coverage towards 100% (98%). Matsumine et al. compared two different treatment approaches for metastatic bone tumors, comprising a group cured by HT treatment and another group where tumors were destroyed by surgery. The results showed that magnetic HT treatment was more effective than surgery alone. In this research, calcium phosphate cement (CPC) containing Fe_3O_4 nanoparticles was reported to have excellent control of metastatic bone lesions [6]. Another clinical study was done by Johannsen et al. on 10 patients with locally recurrent prostate cancer using superparamagnetic nanoparticles. This research showed a drastic decrease in prostate antigen in 8 patients after the magnetic HT treatment [5, 6].

The successful history and significant promising advances in treating cancers by HT and bio-ceramics encouraged us to write this review, which we believe will provide a brief critical assessment of the relevant state-of-the-art. First, some short information about the theory of magnetism in the HT is presented. A comprehensive summary of the synthesis methods and applications, with special focus on cancer therapy feasibility and efficiency by ceramic materials and glasses, is provided. The HT approach for cancer treatment can be used alone or combined with other therapeutic methods like chemotherapy, radiotherapy, phototherapy, gene therapy, immunotherapy, and high intensity focused ultrasound employed in conjunction with HT. Lastly, the opportunities, a view to future work, and challenges are discussed. While the existing reviews in the field are usually quite general and clinically-oriented, the present one is specifically addressed to biocompatible ceramics for HT and their use in conjunction with other anticancer techniques.

2- Basic concepts on magnetism and HT

Knowing about the basic concepts of magnetism will help us understand the mechanism of HT and heat-mediated cancer treatment. Magnetic agents consist of a variety of materials, which are widely used in a range of biomedical applications, especially magnetic resonance imaging (MRI), biosensors, drug delivery, magnetic separation, and magnetic fluid hyperthermia (MFH) [7–11]. Regarding the magnetic responses of the materials in the presence of an external magnetic field, they can be generally classified into ferromagnetism, ferrimagnetism, antiferromagnetism, paramagnetism, and diamagnetism. As illustrated in

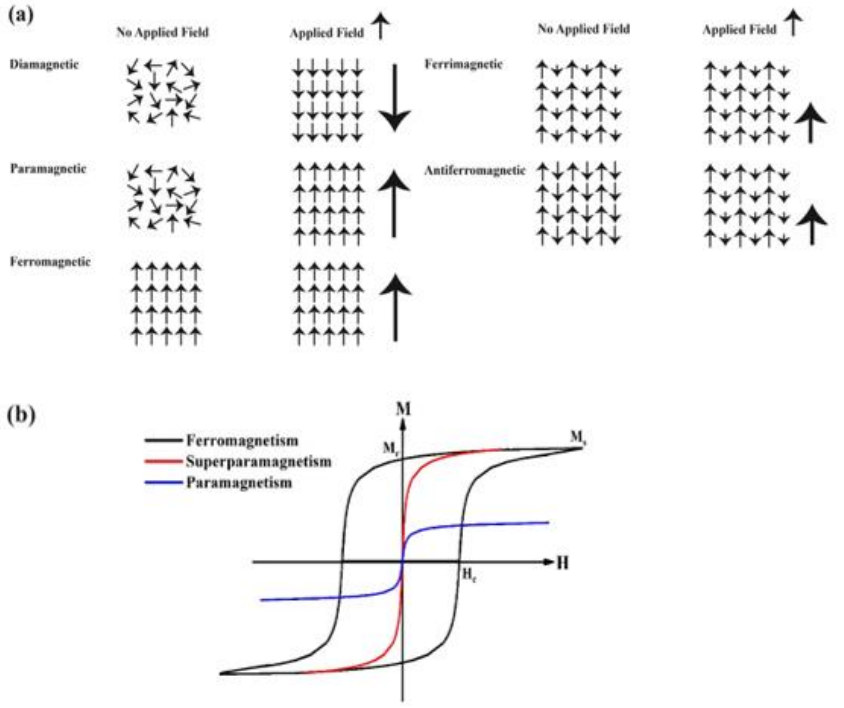

Figure 1a, various magnetic behaviors can be observed in materials exposed to an external magnetic field due to the magnetic orientation of dipoles. In the magnetic field, aligned regions start to either amplify or weaken the initial field. The characteristic magnetic parameters like saturation magnetization (M_s), remnant magnetization (M_r), and coercive force (H_C) of

ferromagnetic, paramagnetic, and superparamagnetic materials shown in

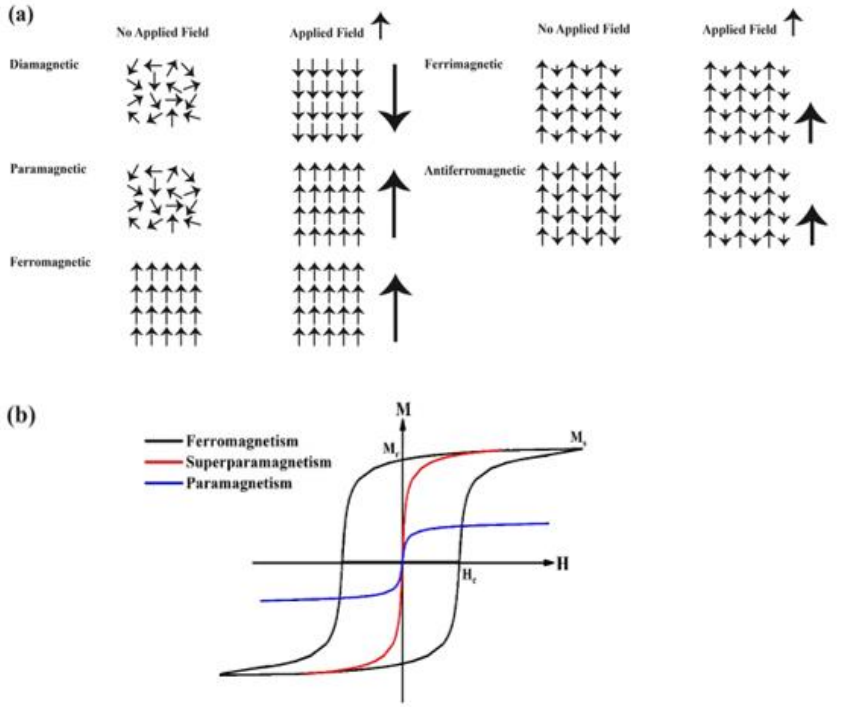

Figure 1b are of great interest for HT.

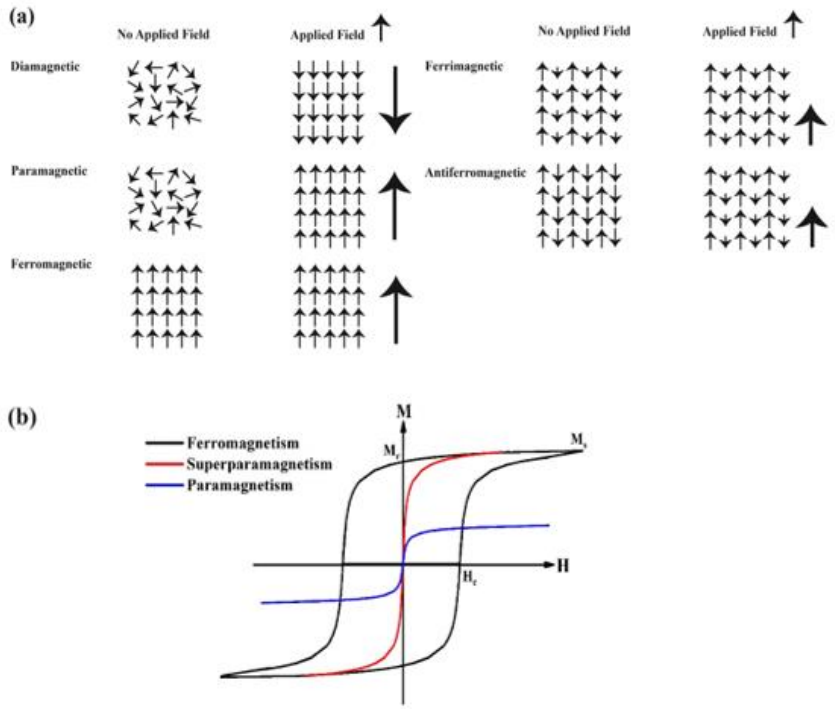

Figure 1- (a) Magnetic moment arrangements in diamagnetic, paramagnetic, ferromagnetic, ferrimagnetic, and antiferromagnetic materials. (b) Hysteresis curve of ferromagnetic, paramagnetic, and superparamagnetic materials.

Due to the near-zero remnant magnetization of superparamagnetic materials, they are superior to the ferromagnetic and ferrimagnetic materials in many applications. Besides, superparamagnetic materials like superparamagnetic iron oxide nanoparticles (SPIONs) can be removed from the suspension and disperse with and without applying a magnetic field, respectively. Additionally, in magnetic HT, the magnetization and reorientation of materials, which lead to energy losses, are significantly important. The area inside the second quadrant of the magnetic hysteresis loop is a good indication of the energy stored in one cycle, which can be used in HT treatment and is affected by the intrinsic and extrinsic properties of materials including magnetocrystalline anisotropy, particle size and shapes, and microstructure. Regarding the hysteresis curve of superparamagnetic materials, no hysteresis losses would be found in these

materials. However, the relaxation time of these particles is more useful for HT heat and energy generation and dissipation. In other words, superparamagnetic behavior has been beneficial in magnetic HT as compared to other types of magnetic materials since the Neel relaxation is more effective than hysteresis losses, which is responsible for temperature rise in superparamagnetic materials [14].

Several features can diminish magnetic materials efficiency in biomedical applications, like aggregation, oxidation, toxicity, high protein absorption, etc. Hence, researchers often employ relatively-affordable surface modification and functionalization strategies to improve some unwanted characteristics and overcome some biological barriers of magnetic materials, especially SPIONs. Several modification agents, such as amino acids, folic acid, polyethylene glycol (PEG), etc., are used to functionalize MNPs via surface treatment, thus shelling the magnetic core with more biologically compatible materials [12–16].

Magnetic properties like H_C M_r and M_s are greatly influenced by size, shape, and surface coating. Due to the core-shell interface and shielding effects of the modification layer, the magnetic properties of the pristine sample will be decreased. Moddy and his coworkers demonstrated the size-dependent magnetic response of magnetic materials [20]. Large magnetic particles consist of several subdomains possessing uniform magnetization and are separated by the walls to reduce the energy of the system. By reducing the materials size, the surface energy of domain walls is becoming more noticeable than the magnetostatic energy. When the materials size decreases below the critical range, the needed energy to create the domain walls becomes higher than the formation of single-domain states. Indeed, by decreasing the size of the particles, H_C will initially increase and subsequently single-domain small particles will reveal near-zero coercivity; therefore, H_C is highly dependent on article size. As a result, MNPs show almost-superparamagnetic behavior, greatly widening their biomedical applications [21].

Additionally, shape anisotropy is another element affecting the materials coercivity. Different synthesis methods lead to various shapes and morphologies like cubic, parallelepiped, cylindrical, or triangular prism [18–21]. Lu et al. demonstrated that the magnetic coercivity of MNPs increases with increasing value of aspect ratio, i.e. when the nanoparticle shape changes

from spherical to elliptical. The H_c reduction is mainly due to the distortion and anisotropy and small deviations from uniformity, which can induce additional anisotropy [22, 23].

The transformation of magnetic energy to thermal energy is measured by the value of the specific absorption rate (SAR):

$$SAR = \mathrm{C}\left(\frac{dT}{dt}\right)\left(\frac{m_s}{m_m}\right) \quad (2)$$

where C is the specific heat capacity of dispersion medium (kcal/kg.^{o}C), $\left(\frac{dT}{dt}\right)$ is the initial slope of the time-heating curve, m_s and m_m are the mass of the solvent and MNPs, respectively. Like the H_c value, SAR is also affected by size, shape, surface modifications, amplitude, and frequency of the AMF. The MNPs with higher SAR have a high potential to be used as MFH [12].

Since there are a few blood vessels and weak vessel networks in cancerous tumors, the need to find a way to destruct cancer cells is becoming widely growing. Up to now, HT is a high-efficiency method to eliminate the cancerous cells at high temperatures (ranging from 41-46 ^{o}C) by using glass and ceramic nanoparticles, which can be transferred through blood vessels [24–27]. The side effects of this method, once properly optimized, are negligible since the mentioned heat is more likely to kill malignant cancer cells, while just few normal cells are damaged at this temperature. HT treatment can be either localized, if microwave, radiofrequency plate antennae applicators or small magnetic seeds are employed, or regional using heated perfusates (hot water) [28–30]. Although the HT method possesses several benefits, it suffers from the difficulty to reach the target temperature and control the localized tumor heating. Another drawback of the HT method is the hard control over avoiding normal cell damage in hardly accessible tumors; in this cases, use of magnetic mediators (fluids) is advised [35].

Generally, based on the magnetic particles used in HT treatment, this method can be divided into four main categories. **Intracellular HT** is a method using rod-like or needle-like MNPs with superparamagnetic properties. In this method, a fluid containing the nanoparticles is injected into the human body and cells can incorporate them by endocytosis. In **extracellular HT**, larger particles (micrometric scale) with ferromagnetic properties, which are stabilized by surfactant in

water, are used. **Magnetic ferrofluid HT** uses ultrafine SPIONs, which are modified with different types of biocompatible agents. Magnetite nanoparticles are commonly used as a mediator of heat when exposed to a high-frequency external AMF. Finally, there is an HT method that uses **magnetic materials in "bulk" form**, which are surgically inserted in the tumor site. The cancer cell death principle in all of these methods is almost the same. Besides being minimally-invasive, MFH has some advantages over the other HT therapy techniques: for example. compared to the NIR laser-based HT, it has better heating efficiency due to the high tissue penetration/enhanced accumulation in the tissues [36] [37].

Owing to the magnetic spins reorientation under an AMF, these materials start releasing heat, which is mainly due to the irreversible magnetization. The other possibility is the rotation of particles in a low viscosity environment causing frictional losses and producing heat in the area. To be more specific, this method mainly involves three steps. Initially, the temperature around the tumor cells and tissues is fixed at about 41 °C. Then, in the second heating cycle, the temperature of the tumor environment will rise to 43 °C and remains constant for a specific time. Finally, although the temperature around tumor tissue may increase, the surrounding normal cells should be maintained at below 46 °C in order to preserve them from thermal damage [37].

3- Materials for HT applications: a short overview

The recent advances in the usage of nanoparticles for HT therapy helped scientists to face many of the challenges of this therapeutic approach, but there are still some concerns. HT therapy can be divided into three main categories for targeting small tissues (local hyperthermia), larger tissues (regional hyperthermia), and all over the body (whole-body hyperthermia). Different types of specific materials should be used for each type of therapeutic method, and each kind of material has its own features, including the amount of heat it can produce, circulation time, and biocompatibility [38]. When nanomaterials are used for HT therapy, three factors play a critical role: high saturation magnetization, low magnetic coercivity, and functionalizable surface. The significance of saturation magnetization and magnetic coercivity has been already discussed in the previous section. Having an active surface allows the attachment of the NPs to the target cells or pathogens selectively. Conjugation of antibodies or

other chemical compounds on the surface of NPs can help scientists to achieve this goal [39]. Having multi-purpose biomedical potential, iron oxide NPs have attracted a huge amount of attention. Gilchrist et al. pioneered the use of magnetic materials for HT therapy in 1965 [40]. They exposed γ-Fe_3O_4 particles to an electromagnetic field to heat tissue samples. They also proved that the heat which was produced by these particles affected the tumor tissue only and no other normal tissues in the body. In addition to iron oxide nanoparticles (IONPs), a considerable number of studies have been conducted on different classes of metallic particles, especially iron (Fe)-based NPs. They have a property that made them very special. These NPs become superparamagnetic at room temperature when their size distribution is below 15 nm [41]. This means that they lose their magnetism as soon as the magnetic field is removed. Therefore, a huge number of studies have been allocated to the usage of metallic alloys, including Fe-Ni-Co, Fe-Au, and γ-Fe-Ni in HT [38–40]. It should be noted that although these NPs show a high magnetic moment, they are toxic and susceptible to chemical reaction or oxidation.

There are two routes to transport the particles to the vicinity of the tumor cells: particles can be injected intravenously and transported by blood circulation or the suspension of particles is directly injected into the desired area. Some of the magnetic NPs (MNPs) mostly have complex synthesis routes, and they tend to agglomerate [45]. Moreover, IONPs have a low circulation time in the body since proteins tend to surround them, and the clearance by the immune system will occur. In order to increase the clearance time and biocompatibility as well as decrease toxic reactivity and oxidation, these NPs are mostly coated/shielded by various kinds of materials, especially biocompatible polymers or ceramics [46]. The problem of obtaining stable aqueous suspensions is typically more critical for metallic NPs than oxide-based NPs [47]. Carbon-based nanomaterials have also been used for a particular type of non-magnetic HT treatment, called photo-thermal therapy. Among these materials, carbon dots have gained more attention. These materials showed low cytotoxicity, and they can be used as imaging agents as well. When these materials are under irradiation of a specific wavelength of light, they will convert it to thermal energy; this process is called photothermal therapy or light-induced HT. In this process, materials with near-infrared (NIR) light adsorptions are the most suitable choices. Therefore, the poor NIR adsorption of carbon-based quantum dots is their main shortcoming. In literature,

several strategies have been proposed to overcome this limitation, such as combination with metallic elements [48].

Recent literature suggests that the last frontier of magnetic biomaterials for HT is represented by functionalized bioceramics, which include iron oxide and its derivatives, calcium phosphate, hydroxyapatite, and glass-ceramics. The magnetic properties and hyperthermia behavior of IONPs have been comprehensively covered in numerous reviews, which interested readers can refer to [?-?] Doping magnetic NPs, coating with bioactive ceramics, and synthesizing a core-shell nano-structure with a magnetic core and a bioceramic shell are the most popular approaches which will be discussed in the present paper. Besides being used as NPs, bioceramics can be embedded in bone cements too [51,52]. These types of magnetic bioceramic cements displayed great ability to fight against cancer cells with no cytotoxicity to healthy cells. In general, glass-ceramics containing magnetic crystals are among the most studied and versatile materials in the context of HT therapy because of their exceptional properties, including good HT properties, bioactivity, and biocompatibility [51]. The results of a study conducted by Ebisawa et al. indicated that the addition of small amounts of Na_2O, B_2O_3, and/or P_2O_5 can induce bioactivity in an otherwise inert and magnetic glass-ceramic material [52]. Moreover, to improve the magnetic and heat generation properties of glass-ceramic materials, different kinds of ferromagnetic crystals, such as zinc ferrite, strontium ferrite, barium ferrites, and so on, were developed by controlled heat treatment within the structure of glass-ceramic materials [49–51]. Li et al. could control the crystallization of Fe_2O_3 and MnO_2 in the structure of glass-ceramic materials. The results were promising [56]; they achieved a biocompatible-bioactive glass, which showed great magnetic properties for HT to treat bone cancer. Therefore, glass-ceramics has the potential to act as multifunctional biocompatible materials with both magnetic and bioactive properties, being able to generate heat for cancer treatment via HT and stimulate tissue regeneration as well.

4- Synthesis methods for bioceramic (nano)particles

Due to the high biocompatibility of most magnetic materials, enormous worldwide attention has been drawn to the use of magnetic nanoparticles for inhibiting cancer cell proliferation via HT [53–55]. The properties of materials, such as physical, chemical, and mechanical characteristics, are significantly affected by synthesis routes. The synthesis method plays a vital role on the size of MNPs, which should be about 20 nm and dispersable in a matrix for generating dipoles in the external magnetic field during magnetic HT, [56, 57]. Bioceramic powders and NPs can be typically prepared by dry-state synthesis, wet chemical methods, and high-temperature routes, as displayed in Table 1Table 1- Comparison of different fabrication methods of bioceramic (nano)powders for HT... In dry-state synthesis, including solid-state reaction and mechanochemical way, precursors are mixed without any solvent. This method is commonly used for mass production, and the chemical compositions of the final products are independent of processing parameters. However, most of the researchers are addressed to wet chemical methods, which allow achieving a high control over the synthesis procedure. Wet chemical synthesis methods comprise chemical precipitation, hydrothermal methods, sol-gel synthesis, microwave-assisted, electrodeposition process, and sonochemical routes. Chemical precipitation is the most famous and popular method to prepare MNPs in biomedical applications since it is a cost-effective and rapid method [58, 59]. Besides, combustion and pyrolysis (slow pyrolysis, fast pyrolysis, and flash pyrolysis) are the main high-temperature methods, in which the NPs are prepared by burning the precursors in the synthesis process. Post-processing treatments, such as surface functionalization, can also be performed to improve the bioceramics characteristics according to each specific application.

Some of the synthesis methods are prone to yield particles with a high tendency to oxidation and agglomeration [60, 61]. The main techniques to prevent these drawbacks are surface modifications, doping with other elements like Cu, Fe, Li, Zn, Mn, etc., and composite development [62–66].

Table 1- Comparison of different fabrication methods of bioceramic (nano)powders for HT.

	Methods	**Advantages**	**Disadvantages**	**Ref.**

Dry-state synthesis methods	Solid-state reaction	Small nanoparticles size, mass production	The need for the high sintering temperature, demanded more processing time	[67, 68]
	Mechanochemical method	Facile method for preparation, high efficiency (high reactant concentrations without using solvent), require low time	Poor crystallinity, the formation of other undemanding products due to competing reaction	[69, 70]
Wet chemical methods	Chemical precipitation	Rapid and simple method, cost-effective method, no need to special apparatus, require low temperature	Poor crystallinity, require high pH, sensitive to the alkali solution, pH, and stirring rate, and sintering temperature	[58, 59, 71, 72]
	Hydrothermal methods	High crystallinity, homogenous powder	Require high temperature, and elevated pressure (P > 100 kPa)	[73, 74]
	Sol-gel synthesis	Possibility of control on the synthesis parameter, high in-vitro, and in-vivo stability	It is costly, generating the second phase	[75–77]
	Microwave-assisted	Require less reaction time, enhanced reaction speed, and high efficiency due to the efficient heat transfer, and kinetic, less power needed	High-cost method and need to special apparatus, improper for mass production	[78–80]
	Electrodeposition	Ultrafine grain nanoparticles, protect metals from corrosion, ability to prepare one-dimensional (1-D) nanomaterials	Time-consuming process, the need for the electrically conductive substrate, need to special apparatus	[85]
	Sonochemical	Uniform size distribution, require less reaction time, ultrafine and pure nanoparticles, high specific area, no need for high temperature and pressure	Need to a certain temperature, need to special apparatus	[86]
High-temperature methods	Solution combustion	Require less reaction time, no need for special apparatus, Possibility of control on the synthesis parameter, ultrafine and pure nanoparticle, high stability, cost-effective method	Presence of a high level of porosity in the final product, wide size distribution, high tendency to aggregate	[87]

	Pyrolysis	Prepare useful production for a wide range of application, high efficiency (75%), require less operation time, Possibility of control on the synthesis parameter	Complex, high-cost method and need to special apparatus, the product gases cannot be sufficiently vented in the cabin	[88]

1-3-2- Scaffolds

The development of advanced biocompatible and bioresorbable scaffold able to mimic the natural tissues constitutes an essential challenge in regenerative medicine. The inherently magnetic scaffold or incorporating MNPs into biocompatible scaffold provides final materials with additional HT functionality. Such a scaffold promises the treatment of critical tissue defects caused by malignant bone cancer through a combined therapy consisting of on-demand temperature increase and, for example, thermally activated drug delivery. There are several potentially useful methods to construct magnetic scaffolds with hyperthermia properties for tissue engineering. Experimental details about the fabrication of a representative set of magnetic scaffolds are summarized here. The following synthesis procedures to magnetize biocompatible scaffolds are widely used in researches, which are discussed in the next sections.

The existence of pathogens or cancer cells in the affinity of organs can cause some severe damage to the organ's tissue. For instance, bone cancer can lead to a defect in the bone structure. In these situations, accelerating the process of cell regeneration is as important as killing the pathogens. Therefore, today scientists are searching for a material that can fight against cancer cells while helping the tissue regeneration process. When it comes to tissue regeneration, scaffolds play a critical role in providing a two- or three-dimensional (2 or 3 D) environment both in-vitro and in-vivo. The structure of scaffolds is designed to have interconnected pores. This structure should provide a stable environment for cell adhesion and proliferation. Among all different materials used as scaffolds, bioceramics are considered a potential candidate [89]. An ideal scaffold should simulate the mechanical structure and biological properties of the original tissues. Studies showed that the biochemical composition of bioceramics could be similar to the native bone structure. Some of the unique properties of bioceramics are osteoconductivity,

bioactivity, biocompatibility, and hydrophilicity [90]. As mentioned before, besides the biochemical properties of scaffold, its structure plays an essential role. Using an appropriate synthesis method and designing the hierarchical structure with suitable porosity, pore size, which allows cells to spread, and interconnected pores are the factors that shape an ideal scaffold. Scaffolds with micro or nano-structure benefit from higher surface area and roughness, increasing the adhesion between the structure and cells [91]. Different synthesis methods have been proposed to achieve the ideal scaffold structure. The main aim of all these approaches is to increase the control of the micro or nanostructure of the scaffolds. Each technique is designed to achieve a specific range of structural properties, including distribution of pores, pore size, and so on. Moreover, each method's overall cost and scale of production differs from another one [92]. The main aim of this section is to summarize all the techniques used to synthesis bioceramic scaffolds. Fabrication methods can be divided into two leading groups: conventional methods and additive manufacturing. Conventional methods include foaming methods, starch consolidation, organic phase burning out, polymer replication method, solid freeform fabrication, and freeze-drying. In most of these techniques controlling the pore distribution, pore size or interconnectivity, and geometry of the pores is either very difficult or not possible. Therefore, it is hard to specifically adapt the scaffold’s properties to enhance cell growth and tissue engineering. To overcome these shortcomings, scientists developed another state-of-the-art method, called additive manufacturing. 3D printing is a subgroup of additive manufacturing that attracted a tremendous amount of attention. Body tissues, especially bone tissue, have complex porous structures, which was very hard to achieve before using the 3D printing method [89–92]. This method enables scientists to precisely synthesize a structure, which mimics the tissues' structure, stimulates nutrient transport, cell migration, and facilitates the regeneration process [97]. All these techniques have been discussed in detail in the literature [85, 94, 95]. Table 2 summarized the most notable advantages and disadvantages of some of the most commonly used methods for synthesizing a highly porous scaffold from bioceramics.

Table 2 Comparison of different fabrication methods of bioceramic scaffolds

	Methods	Advantages	Disadvantages	Ref.

Conventional methods	Foaming methods	H_2O_2 Foaming	A simple method, no need secondary phase as a porogen, avoiding impurities contamination from porogen producing only water as a by-product,	Low porosity control, hard to achieve a 3D structure with interconnected pores. (Almirall et al. and Huan et al. suggested ways to synthesis interconnected bioceramic scaffold.)	[96–99]
		Sol-gel Foaming	Hierarchical structure with interconnected macropores and a mesoporous texture, which is suitable for cell adhesion and proliferation	High degree of control is required	[100–102]
		Gel-cast Foaming	Complex shaping capability, good dimensional accuracy, thick walls with homogeneous micro-structure, and high strength	Low pore interconnectivity	[103, 104]
	Organic phase burning-out		High mechanical properties	Hard to achieve a structure with interconnected uniform pores	[109]
	Polymer replication method		Highly porous structure with uniform interconnected pores,	Poor mechanical straight due to the existence of sharp apices that commonly present at the center of the hollow struts due to polymer burnout	[106, 107]
	Freeze drying		Highly porous, cost-effective	Small pore size, long processing time, and low pore size distribution	[106, 108]
Additive manufacturing	3D Printing		Fast processing, great control on the structure, tunable mechanical properties, good interconnectivity, complex scaffolds can be fabricated	Trapped powder issue	[89, 93]
	Selective laser sintering (SLS)		Good mechanical properties, high accuracy, multiple materials can be processed in a single bed	A process with high temperature, hard to remove a trap powder, slow, expensive, rough surface	[85, 109]

5- Researches on crystalline bioceramics for magnetic HT

As it was mentioned before, there is a high risk of toxicity for, iron oxide and metallic alloy magnetic nanoparticles used as such. Therefore, doping and coating strategies as well as the development of core-shell nanostructures have been proposed to improve biocompatibility while the final product could still benefit from the great magnetic properties of magnetic NPs. Ruthradevi et al. [114] reported a core-shell structure with the core of nickel ferrite NPs as the magnetic source and a shell of calcium phosphate. The final product performed superparamagnetic behavior with zero coercivity at 300 K and ferromagnetic behavior with a coercivity of 0.045 T at 5 K. It was reported that the final product was biocompatible, although it could not reach the desired temperature to kill the cancer cells; therefore, further optimization is required. In another study, Fe^{3+} was incorporated into hydroxyapatite NPs, and the samples reached the maximum temperature of 48 °C in 10 min during induction heating tests [115]. Adamiano et al. [116] synthesized two superparamagnetic nanocomposites of iron-doped hydroxyapatite (FeHA) and iron-oxide NPs coated with amorphous calcium phosphate (Mag@Cap). Magnetometry results revealed that specific saturation magnetizations of FeHA and Mag@Cap were almost 4 and 5 emu/g, respectively. TEM images of the as-synthesized materials were shown in Figure 2(A-E), and the core-shell morphology of Mag@Cap NPs and the needle shape morphology of the FeHA are visualized in these pictures. Agar assays were used to test the antibacterial effects of the samples, and no activity was discovered against Gram-positive and Gram-negative bacteria. Figure 2(F) illustrates that once cancer cells were allowed to uptake the FeHA and Mag@Cap NPs and the AMF was employed, the cancer cells viability has been lessened considerably. Fluorescent microscopy images were used to confirm the uptake of iron-containing NPs into E297 and K7M2 cells; specifically, 44.9 ± 12.0% of cells incorporated FeHA NPs and 17.7 ± 1.6% of cells internalized Mag@CaP NPs. Another research was conducted to study the in vivo performance of magnetic hydroxyapatite (mHAP) NPs for HT therapy [117]. Doping with Fe^{2+} was performed to induce magnetic properties in hydroxyapatite NPs, which were then mixed with phosphate buffer solution (PBS) and injected around tumor cells. An alternating magnetic field was used to increase the temperature and, after 15 days of observation, remarkable reduction of tumor volume was seen in the mice which were injected with mHAP. In a recent study, maghemite (γ-Fe_2O_3) NPs were synthesized and embedded in a

nanohydroxyapatite (HAp) matrix (GFeHAp) using the co-precipitation method [118]. An experiment under AC magnetic fields was carried out to study the heat-generating properties of the final particles. The results showed that, when the concentration of NPs in water reached 20 $mg.mL^{-1}$, the temperature increased to 45 °C during 10 min. Human (Sarcoma osteogenic) SAOS-2 cell lines were used to study the biocompatibility of these NPs. Results were promising and showed that the addition of maghemite to HAp does not induce any cytotoxicity in the final NPs, even when 125 μg $mL^{-1}$of the NPs were incubated with the cells for 24 h. In this article, it was also reported that the NPs showed small coercive fields in the M-H loops and, after functionalizing the NPs, H_c still showed the same value (H_c = 70 Oe). Moreover, the values of saturation magnetization (M_s) for GFeHAp was around 12 emu g^{-1}, which was less than the M_s of the bare maghemite NPs and revealed that the synthesized NPs were not superparamagnetic. This was suggested to happen because of the size of NPs, which was above 10 nm. Although also these bioceramics NPs showed promising properties for HT applications, further studies are required to produce NPs with even better magnetic and biocompatibility properties.

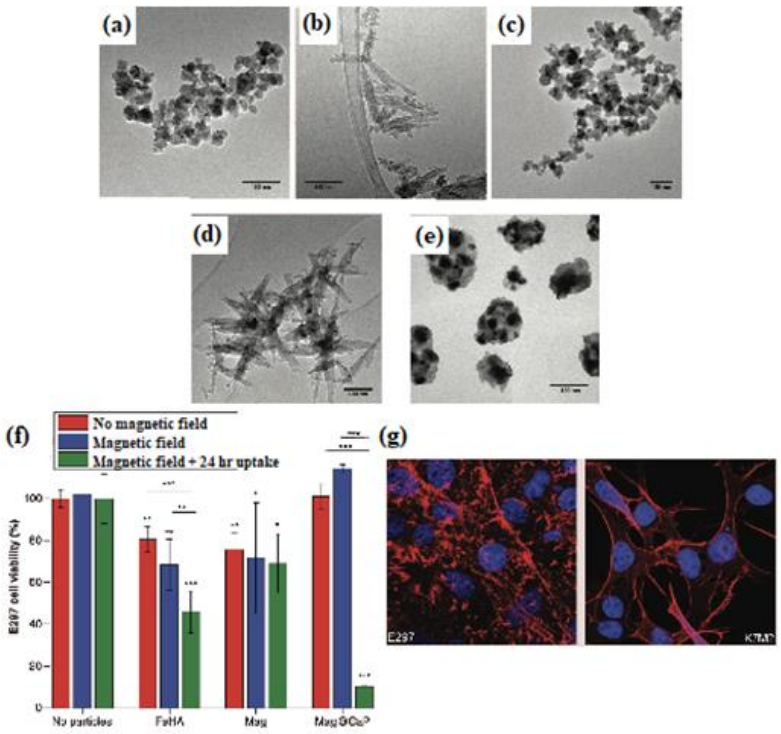

Figure 2- (a) TEM images of iron oxide, (b) hydroxyapatite, (c) calcium phosphate, (d) iron-doped hydroxyapatite and (e) iron oxide nanoparticles coated with amorphous calcium phosphate. Viability of human E297 glioblastoma cells after the alternating magnetic field (300 kHz, 1.16 μT) treatment for 30 min. (f) Data points are shown as averages (n = 4–8) with error bars representing the standard deviation. (g, h) Immunofluorescent images of cells in interaction with iron oxide nanoparticles coated with amorphous calcium phosphate. Fluorescently stained E297 glioblastoma and K7M2 osteosarcoma cells (cytoskeletal f-actin – phalloidin; nucleus – DAPI) display no adverse effects on their proliferation degree or morphology following the 24-h treatment with 10 mg/ml iron oxide nanoparticles coated with amorphous calcium phosphate [116].

6- Researches on bioactive glasses and glass-ceramics for magnetic HT

The final goal of any cancer therapy method is to kill the cancer cells entirely while irreversible damage to healthy tissues is minimized. During therapeutic treatment, however, some damages to healthy cells are inevitable. In this case, it is of chief significance to develop and choose a bioactive material that can simultaneously (i) foster tissue regeneration to help the healing process and (ii) have good properties for HT therapy to kill cancer cells or pathogens. The composition of biocompatible glasses and glass-ceramics can be properly designed so that they can facilitate tissue regeneration, especially bone, while having an excellent HT effect. When these special biomaterials, called bioactive glasses (BGs) and glass-ceramics (BGCs), are implanted in the body, chemical bonds between the implant and the living host tissue are formed by the precipitation of an interfacial apatite layer on their surface [119]. BG and BGCs can stimulate several favorable responses in the body, including bone-bonding ability, bone regeneration, regeneration of soft tissues, bactericidal effect, therapeutic ion release, angiogenesis, drug delivery, high mechanical support (e.g. tough BGCs), and cancer therapy like magnetic HT [120–122]. As an example, it was observed that the addition of certain oxides to the structure of a glass-ceramic material (FeO-Fe_2O_3-CaO-SiO_2) could induce bioactivity in the final material [123]. In the study conducted by Qi et al., 3D printing technique was used to synthesize a calcium sulfate hydrate (CSH)/mesoporous bioactive glass (MBG, Si/Ca/P molar ratio 80/15/5) composite scaffold for bone tissue engineering [124]. This scaffold had a uniform macroporous structure with high porosity and the ability of apatite mineralization. When this scaffold was incubated with human bone marrow-derived mesenchymal stem cells (hBMSCs), gene expression and cell proliferation were exhibited. As shown in Figure 3, cell proliferation, alkaline phosphatase activity and gene expression were increasingly stimulated by increasing the MBG addition. In-vivo results also proved that this BG-based scaffold could stimulate cell adhesion and proliferation, leading to the expression of osteogenesis-related genes. Results from micro-tomographic analysis also confirmed that the presence of MBG could enhance bone regeneration in rats [112].

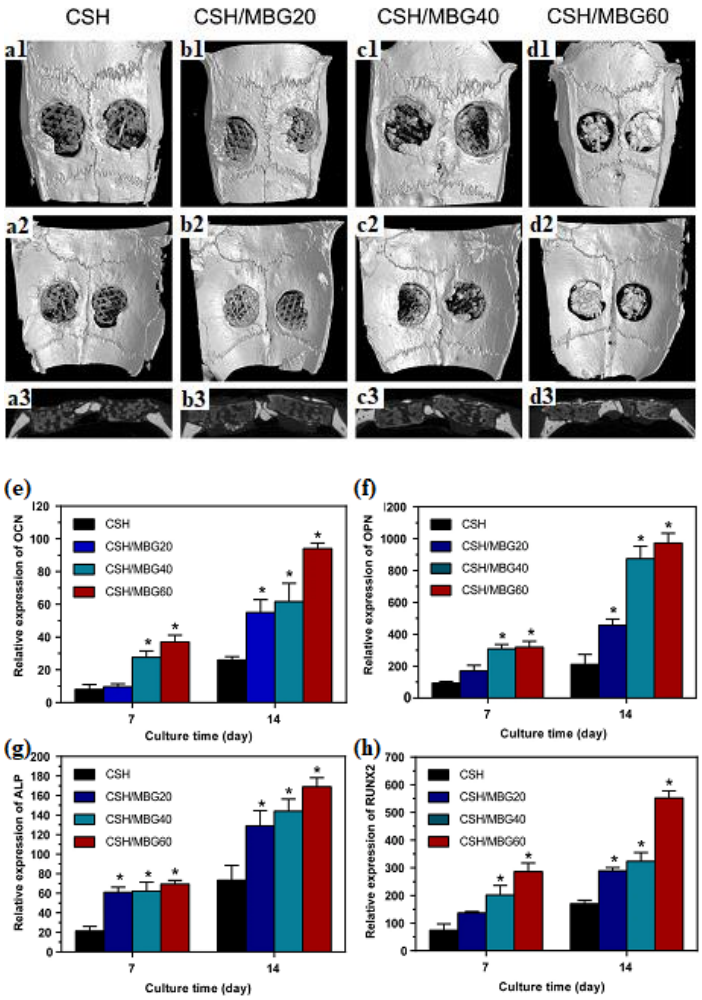

Figure 3- (a1-d1) Morphometric analysis and Micro-CT evaluation of calvarial defect bone repair. Pictures were taken after eight weeks of scaffold implantation. 3D superficial, (a2-d2) interior images, and (a3-d3) sagittal images of calvarial bone defects. (e) Osteogenic expression of OCN, (f) OPN, (g) ALP, and (h) RUNX2 for hBMSCs cultured on the CSH and CSH/MBG scaffolds by qRT-PCR analysis after 7 and 14 days (n = 3; *indicated significant differences when compared to CSH, $P < 0.05$) [112].

Unlike iron oxide NPs, BGs and BGCs do not usually show a magnetic behavior unless magnetic phases are embedded in their structure. Li et al. [ref] firstly synthesized a magnetic and mesoporous BG by homogeneously dispersing Fe_3O_4 NPs in the mesoporous glassy matrix. Addition of Fe_3O_4 NPs to the structure induced superparamagnetic properties in the BG, while it did not negatively affect the textural properties. Luderer et al. were the first ones reporting the use of a glass-ceramic for HT cancer therapy [125]. In another study on the HT application of a glass-ceramic ($CaO–SiO_2–Fe_2O_3$) system, the magnetic oxidation was restricted using a controlled two-step crystallization of magnetic crystals [126]. An important goal of that work was to avoid the presence of undesired non-magnetic phases, thereby enhancing the heat-generating power of the final system. Ji et al. produced quaternary $P_2O_5–Fe_2O_3–CaO–SiO_2$ (PFCS) glass-ceramics as potential materials for HT [127]. The samples showed very low cytotoxicity while they exhibited great heat-generating ability. One of the samples reached the death rate of 95% for LoVo cancer cells. This study also proved that the amount of phosphorus could affect the crystal phase composition of the as-prepared samples. Hence, the content of phosphorus has an impact on the heat-induction ability. Baino et al. [ref] used a sol-gel method to synthesize a Fe-doped BG and proved that the addition of Fe_2O_3 into a binary $SiO_2–CaO$ parent glass could induce good magnetic behavior in the as-synthesized materials. Foaming methods incorporated in the sol-gel process also allowed fabricating porous hierarchical scaffolds based on these materials [ref].

The addition of ferromagnetic NPs into glass-ceramic materials raises a concern about the possibility of exposing ferromagnetic NPs, which might negatively affect the biocompatibility and bioactivity of glass-ceramics. Recent studies showed that, interestingly. encapsulation of magnetite NPs in the glass matrix allows Fe^{3+} ion leaching to be prevented [128]. Specifically, the interfaces between magnetite and three popular BG systems, $80SiO_2–15CaO–5P_2O_5$ (80S), $58SiO_2–36CaO–6P_2O_5$ (58S), and $35SiO_2–50CaO–7P_2O_5–7MgO–1CaF_2$ (35SM) in mol.%, were investigated [129]. This study reveals that Fe moves much faster to the glass phase than Si transfers to the ferrite phase. Moreover, the diffusion rate of the Fe to glass phase is not the same in all the samples. For instance, among all the studied samples, migration of Fe from NPs to glass is much easier in the interface of sample 58S. In another research, copper was added along with iron to the structure of the glass [130]. The results of this study reveal that addition of

copper oxide to the structure allows enhancing the magnetic saturation of the final product while concurrently reducing the amount of required Fe to obtain the same effect. In this study, three samples were synthesized by the sol-gel method: 1) BG with Fe (FeBG), 2) BG with Fe and Cu (FeCuBG), 3) BG with Cu (CuBG). Among all these samples, FeCuBG showed the greatest superparamagnetic behavior (Figure 4b). The magnetic properties were investigated under a magnetic field of 20000 Oe for all samples. The saturation magnetization of FeCuBG was almost five times that of the sample without Cu. An ICP analysis shows that the amount of Fe released in SBF is negligible, which is due to its strong bonding in the glass structure. Figure 4a represents the pH of samples in the SBF, which is in the range of 7.0 to 7.9. This range of pH (moderate alkalinity) plus the low release of Fe result in a suitable condition for adhesion and growth of cells. In-vitro analysis shows that the cytotoxicity of FeBG and FeCuBG is lower than that of CuBG (Fig 4c). However, the samples containing Fe show a lack of HUVEC cell proliferation in comparison with control samples (Fig 4d). Altogether, since magnetic BGCs benefit from both bioactivity and good magnetic properties, they have a terrific potential for HT therapy applications.

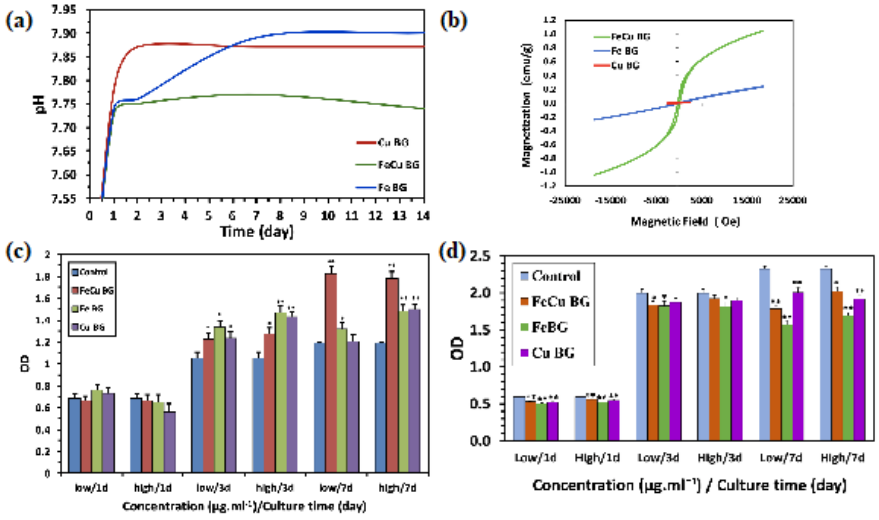

Figure 4- (a) The pH diagram for different samples after soaking for a different amount of times in SBF, (b) VSM graphs, (c) MTT assay of bioactive glasses, along with negative and positive controls with two concentrations (low: 200 $\mu g.mL^{-1}$ and high: 400 $\mu g.mL^{-1}$) for 1, 3 and 7 days,

(d) HUVEC proliferation under exposure to the bioactive glasses with controls at two concentrations (low: 100 μg.mL^{-1} and high: 200 μg.mL^{-1}) for 1, 3 and 7 days (d). [The mean difference compared to the control group is significant at the 0.05 level (*) and 0.001 (**)][130] .

Table 3 summarizes some of the studies on the application of magnetic glass-ceramics for cancer therapy. The parent glasses are prepared by melting or sol-gel routes. After controlled heat-treatment of the parent glasses, the magnetic phases are crystallized while residual glass phase provides bioactivity [54,117,132–136,119,125–131]. Magnetic crystals include lithium ferrite ($LiFe_5O_8$), magnetite (Fe_3O_4) Zn ferrite, Li-Mn ferrite, Mg ferrite, Mn-Zn ferrite, $BaFe_{12}O_{19}$, $SrFe_{12}O_{19}$, etc. For example, the transmission electron microscope (TEM) image in Figure 5 shows ferrite nanocrystals surrounded by the residual glass and a β-wollastonite phase [142].

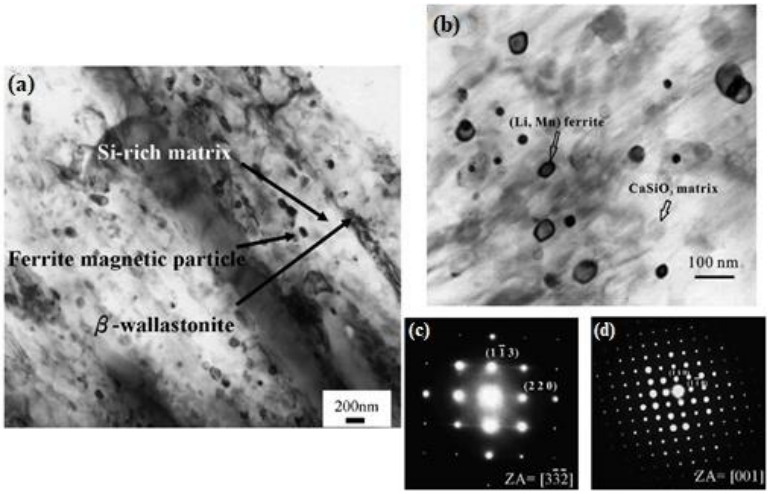

Figure 5- (a) TEM micrograph of the $25Li_2O–8MnO_2–20CaO–2P_2O_5–45SiO_2–4Fe_2O_3$ ($at.\%$) glass crystallized at 850 °C for 4 h. (b) Bright-field images and (c) SAED pattern of the (Li,Mn) ferrite with the $[3\bar{3}\bar{2}]$ zone axis and (d) β-wollastonite with [001] zone axis [142].

Generally, iron in the glass composition should remain in the crystal structure because, otherwise, it would diminish the apatite-forming ability of the residual glass matrix. In order to

satisfy this criterion, biphasic materials containing a melt-derived magnetic glass-ceramic ($45SiO_2$–$45CaO$–$10Fe_2O_3$ in mol%) and a gel-derived BG ($58SiO_2$–$6P_2O_5$–$36CaO$ in mol%) were suggested by Vallet-Regí's team [137–139]. The sol-gel BG exhibits an inherent nanoporosity, which plays a fundamental role in promoting the apatite-forming ability on the surface [143]. On the other hand, as the sol-gel BG content increases, the magnetic properties change due to the diffusion of Fe ions to the glassy phases of the biphasic materials. Additionally, the biphasic nature of these materials allows proper modulation of both properties, depending on the patient's requirements [137–139].

Magnetic glass-ceramic powders can also be included in polymer-based bone cements [ref].

Commentato [F1]: Check these ref as numbering is incorrect.

Commentato [F2]: Add ref here

Table 3 The summary of the studies on the magnetic bioactive glass-ceramics for cancer therapy application. Can you add another column showing the crystalline phases of the GCs? These crystals stimulate HT and are important.

Material	preparation	Magnetic properties		Bioactivity / Biocompatibility	Other features	Ref.
		Saturation magnetization (emu/g)	Coercive force (Oe)			
$40SiO_2$-$10Li_2O$-36-CaO-$4P_2O_5$-$10Fe_2O_3$ (mol%)	Sol-gel	8.297	29	-/-	Four other composites were synthesized in this study, but the mentioned composition exhibited the best properties. The mentioned composite creates enough heat to kill cancer cells.	[146]
CaO-SiO_2-MgO-CaF_2-P_2O_5-Fe_3O_4	Sol-gel	10.6 (Am^2Kg^{-1})	-	After soaking in simulated body fluid (SBF), the formation of an appetite layer containing carbonate on the surface of graphite modified Fe_3O_4 was observed / No cytotoxicity for VX2 cells	The Fe_3O_4 was protected from oxidation by the addition of graphite. The as-prepared material was bioactive and showed good heat generation ability.	[147]
$13Fe_2O_3$-49CaO-	Sol-gel	-	-	Addition of P_2O_5 increase the	During soaking in SBF, the	[148]

$xSiO_2$ yP_2O_5 - $zTiO_2$ (mol%)				formation of carbonate hydroxyapatite layer on the surface of the sample while soaking in SBF / P_2O_5 addition decline the cytotoxicity to FHC cells	weight of the sample didn't decrease (showed stability)	
47.5SiO_2- 20CaO-10MgO- 2.5P_2O_5-10K_2O-10Na_2O (mol%)	Sol-gel			After two days of immersion in SBF, apatite-like structures were observed to form. / -		[149]
Shell: SiO_2-CaO Core: γ-Fe_2O_3	Co-precipitation and sol-gel	57±1 (at 300 K)	-	After immersing in the SBF, a layer of hydroxyapatite was formed on the surface/results of MTT assay, showed no significant change in the activity of h-MSC[1] cells	Have a good heating capacity, heterostructures are not agglomerated, AMF results showed that NPs induced enough temperature in water to have a therapeutic effect on cancer cells	[150]
(100-x)(58SiO_2-	Sol-gel	1.91-3.49	-	Calcium and phosphorus phases	The composites with x=10 & 20,	[151]

[1] Human mesenchymal stem cells

33CaO- 9P_2O_5)-xFe_2O_3 (x=10,20, & 30 wt.%)				were formed on the surface after immersing in SBF / low cytotoxicity at a low concentration	showed hysteresis with low M_R[2]and H_c[3]. the x=30 composite showed no M_R and H_C (superparamagnetic behavior)	
46.1SiO_2-21.9CaO-24.4Na_2O-2.6P_2O_5-5SrO (mol%)	Melt quench	5, 7, and 10	-	After SBF treatment, the precipitated hydroxyapatite phase grew on the surface/exhibit excellent biocompatibility toward human osteosarcoma MG63 cell lines	Composites showed an antibacterial effect on the E.coli and S. Aureus bacteria cells. These samples showed room temperature superparamagnetic behavior as well as suitable heating ability.	[152]
(45-x)CaO-34SiO_2- 16P_2O_5-4.5MgO- 0.5CaF_2- - xFe_2O_3 (x=5-20 wt%)	Melt quench	0.21-8.89	149-575	Bioactivity increased by further iron addition / -	Higher concentration of iron improved crystallization degree of magnetic phase	[153]

[2] Residual magnetization
[3] Coercive field

BGCs can be used for both magnetic HT and photo-induced (photothermal) HT. Given the importance and great potential of the latter approach, a short description of this HT therapy is provided here for the Reader's benefit. As it was mentioned before, materials designed to be used for photothermal therapy should reveal NIR absorption peaks. This feature will help them to achieve maximum radiation penetration into the tissue. Wang et al. [154] developed a Bi-doped BG for photothermal application with adsorption peaks around 700, 800, and 1000 nm. These peaks were absent in the samples without Bi. When the samples were under laser irradiation, un-doped samples showed no significant temperature variation. In contrast, Bi-doped samples showed temperature variation from 54 to 223 °C. Figure 6a illustrates that the highest temperature is achieved when the highest dopant concentration was added to the structure. The toxicity of these Bi-doped phospho-silicate glasses (S6PyB) was examined by in vitro tests with mouse fibroblast cell line (L929), murine calvarial pre-osteoblast (MC3T3-E1) cells, rat osteosarcoma-derived (UMR106) cells, and human osteosarcoma (U2OS) cells. Generally, the cell viability was more than 80% for all types of cells (Figure 6b). Figure 6c displays the mineral deposits formed on the surface of the materials when they were immersed in SBF. For samples with a higher concentration of Bi, after 7 days immersion, the initial surface microstructure transformed into an assembly of plates. Rod-shaped clusters, which facilitate the corrosion reaction, are not observed even after 12 days for the sample with the highest Bi concentration. In-vitro mineralization of osteoblast cells showed the higher calcium deposition on the surface of Bi-doped glasses. In-vivo results in a mouse model were also promising: Figure 6d shows that a significant difference exists in tumor size reduction between the control sample and the mice receiving Bi-doped BGs under laser irradiation [154].

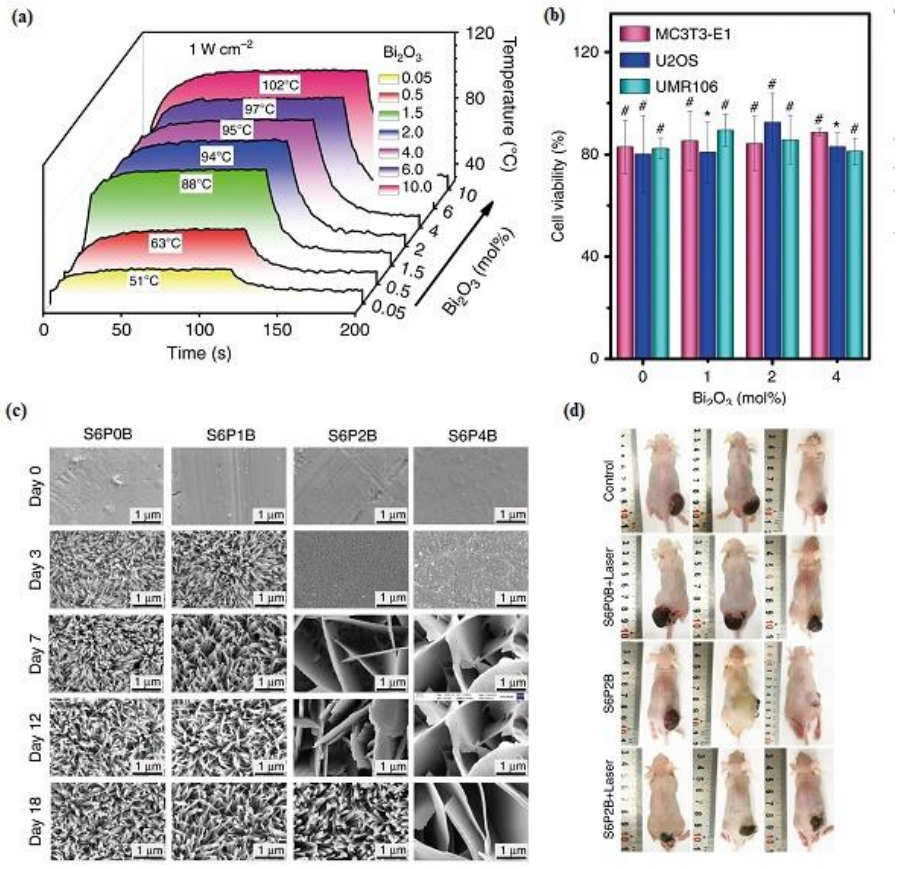

Figure 6- (a) Temperature curves of Bi-doped glasses as a function of irradiation time; power density of 808 nm LD was attenuated to 1 W cm^{-2}. (b) Viability of normal cell MC3T3-E1, and tumor cells of human osteosarcoma line U2OS and rat osteosarcoma cell lines UMR106 after co-culturing with S6PyB; data points represent the mean values and error bars according to three independent experiments. (c) Morphological evolution of glass samples S6PyB as incubated in SBF for different days as indicated. (d) Images of mice in "control", "S6P0B + laser", "S6P2B" and "S6P2B + laser" groups at day 15 (d) (SxPyB :(49-x-y) SiO_2-24 Na_2O-27 CaO-x P_2O_5-y Bi_2O_3 (x = 0, 2, 4, 6, 8, 10 , y = 0, 1, 2, 4, 6) [154]

7- HT in conjunction with other techniques

Cancer treatment is often performed by applying multiple treatments, being surgery followed by chemotherapy and/or radiotherapy the most common combinations. Following this line of action, the development of multifunctional bioceramics for cancer treatment has been showing great promise to increase therapeutic success. Specifically, special ceramics and glasses able to elicit HT effect in combination with anticancer drug local release or photonic nanomedicine have been investigated over the last five years.

7-1- HT combined with chemotherapy (drug delivery)

Drugs can be introduced into the body via different methods. Nanotechnology has significantly transformed chemotherapy methods and made it possible to expose the predicted amount of drug with the expected rate just into the target sites like cancer cells. After using nanotechnology for drug delivery, an increase in the effectiveness of chemotherapy methods and reduction of the relevant side effects have been observed. During the past few years, the idea of using nanomaterials for both HT therapy and drug delivery has drawn more and more attention. Scientists are trying to develop a system that is able to treat cancer cells with both HT technique and chemotherapy. In this way, cancer cells will be synergystically attacked by both heat and drugs. When heat is generated in the microenvironment of cancer cells, less amount of drug is required for killing them. Therefore, the development of a bioactive and biocompatible system with great HT and drug delivery properties would be an exceptional milestone in cancer therapy. Among bioceramics, magnetic mesoporous silica has shown great potential to be used as a platform for both chemo- and hyperthermia therapy. However, there are two issues related to these NPs: burst effect and protein corona. In this regard, such NPs are mostly coated with polymeric materials. When a magnetic bioceramic is heated by AMF, and this ceramic is coated with a thermally-responsive polymer, the heat generated by HT can trigger drug release, which could substantially increase the efficiency of killing the cancer cell. Tian et al. [155] coated magnetic mesoporous silica nanoparticles (MMSNs) with a thermo-responsive copolymer (MMSN@P(NIPAM-co-MAA)). They dispersed 1.0 g of Fe_3O_4 nanoparticles in 90 ml of water: for this purpose, 1.71 g of CTAT and 1.0 g of TEA were added and stirred vigorously at 80 °C until they dissolved completely. Subsequently, 14.0 ml of TEOS was rapidly added to the above

solution and the mixture was allowed to react for 2 h. Brown colloidal nanoparticles were separated with a magnet, washed several times with ethanol, and dried in vacuum at 60 °C for 24 h. Finally, MMSNs were obtained after calcination of dried brown colloidal nanoparticles at 540 °C for 7 h. Then, the MMSNs were coated with the P(NIPAM-co-MAA) copolymer and the final product exhibited a superparamagnetic behavior with a saturation magnetization of 6.2 emu/g. Doxorubicin hydrochloride (DOX), as an anticancer drug, was loaded to the MMSN@P(NIPAM-co-MAA) that displayed a temperature- and pH-responsive drug release. Results showed that the rate of drug release had been accelerated by HT-induced temperature increase and low environmental pH, which yielded higher efficiency in killing cancer cells. Moreover, when the as-synthesized NPs were incubated with HeLa cells, they did not show notable cytotoxic behavior, and cells could uptake NPs efficiently. In another study, a core-shell structure of mesoporous silica NPs with the core of iron oxide (Fe_3O_4) was coated with poly(carboxybetaine methacrylate) (pCBMA) [156]. In order to evaluate the suitability of these NPs for drug delivery, an anti-breast cancer drug (Tamoxifen) was loaded to the NPs; results proved that Fe_3O_4@mSiO2@PCBMA had a stable drug release with less than 20% of the drug released in the first 24 hours, demonstrating that the problem of burst effect had been overcome. Furthermore, MTT results displayed no significant cytotoxicity.

Guisasola et al. [157] embedded magnetite (Fe_3O_4) in the mesoporous silica matrix and coated the final product with a thermosensitive polymer. Figure 7 (A) illustrates the structure of the final product and the core-shell structure of this nanocomposite has been displayed by TEM image (Figure 7 (B)). Like other studies, they could reach a synergistic effect between heat generation of HT and drug delivery, which can lead to injecting less materials and using milder AMF parameters. As shown in Figure 7 (B, D, E), after being injected, the NPs have deeply penetrated into the cancer cells. Results also proved that the tumor volume of the control was doubled from day 3 to day 5 of the experiment, whereas the tumor growth for the group receiving complete treatment with the synthesized material has been inhibited.

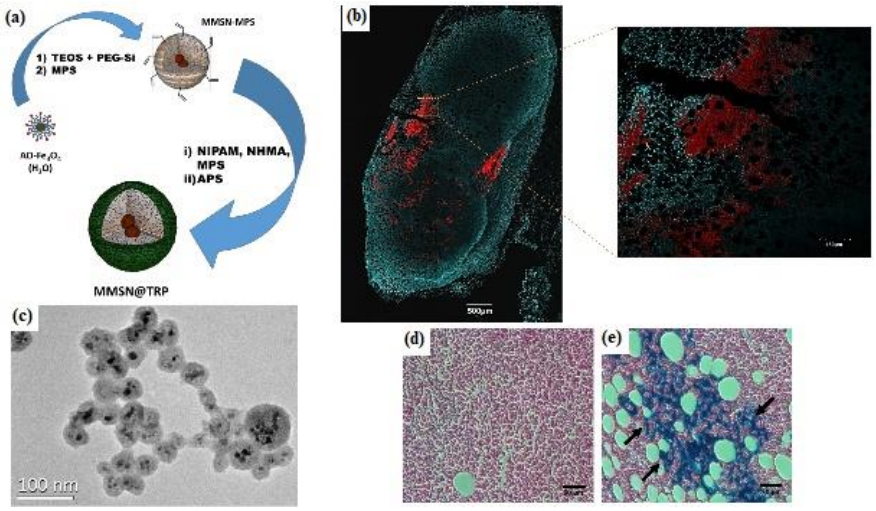

Figure 7- (a) Scheme of the synthetic route, (b) Confocal images of tumor slices after being stained with DAPI. Red fluorescence came from the Rho-nanocarriers, (c) TEM images of the NPs, (d) Perls staining (blue) of tumor slices from Control mice without nanocarriers, (e) and mice tumors injected with nanocarriers. The scale bar corresponds to 50 μm. In accordance with the diffusion studies, great results of tumor growth inhibition were obtained. Arrows indicate the presence of iron.

Some mesoporous materials, like MBGs, have also been proposed as such (without polymeric coating) for combined treatment of cancer via magnetic HT and chemotherapy. In this regard, Wu et al. reported the use of foam-like Fe-doped MBG scaffolds as multifunctional implants for inducing cancer cell death via magnetic HT effect plus local drug delivery and for concurrently stimulating bone regeneration [ref].

Some types of non-mesoporous magnetic bioceramics have also shown promise for use in chemo-thermal cancer therapy. For example, Luo et al. synthesized SiO_2–CaO–Fe_2O_3 (SCF) glass-ceramic hollow nanospheres (GCNS) by a sol-gel technique [160]. The obtained results showed that crystallization, morphology, and magnetic properties of the SCF-GCNSs depended on the redox state and composition of Fe precursors. When the amount of Fe_2O_3 was less than 15 wt.% the morphology of SCF remained spherical; on the contrary, the morphology of SCF-GCNSs changed and became crashed and aggregated with increasing amount of Fe_2O_3, Crystallization of magnetite phase was promoted when the ratio of $FeCl_3$/$FeCl_2$ precursors in

glass preparation was increased, thus directly affecting the magnetic performance of SCF-GCNSs. When the precursor ratio of $FeCl_3$:$FeCl_2$ was 2.5:1, the saturation magnetization and coercivity of the sample were 254.14 Oe and 2.51 emu/g, respectively. The drug delivery properties were also investigated, revealing a large drug loading capacity (24.2 wt.%) and sustained drug release behavior up to 100 hours.

Non-porous NPs were also proposed by Seyfoori et al. [159] who synthesized $ZnFe_2O_4$ and $ZnFe_2O_4$–hydroxyapatite nanostructures by co-precipitation method. Analysis of magnetic properties proved that the sample with hydroxyapatite had lower saturation magnetization and higher coercive field, which aids adhesion and proliferation of cells. When these nanoscale materials were loaded with drug as a nanocarrier, they displayed inhibitory effects on the proliferation of G292 cancer cells while the proliferation of HEK normal cells was stimulated. Recently, MNPs were encapsulated in the bioactive glass structure for bone-related cancer treatment application. The co-precipitation method was used to synthesize MNPs, and then the sol-gel technique was used to embed them into bioactive glass structure. The bioactivity of the final product was illustrated by the formation of a hydroxyapatite layer on the surface of samples. Biocompatibility of the particles was studied by their incubation with human osteosarcoma cell line (MG63) and displayed no cytotoxicity. Under the AMF, the temperature of the particles had raised to 42 °C. Before loading the drug on the synthesized particles, the surface of bioactive glass-ceramics was modified to increase the functional group on their surface, which leads to enhancing the drug load ability of the biomaterial. Doxorubicin (DOX) was loaded to magnetic bioactive glasses and showed sustained release of the drug. These studies provides evidence that developing biocompatible/bioactive bioceramics as multifunctional agents for drug delivery and magnetic HT can actually be a powerful approach to combat against cancer cells, especially bone cancer cells.

7-2- Radiotherapy

A few research studies have been reported on materials able to perform HT and radiotherapy simultaneously. Apart from chemotherapy, the other primary non-invasive therapeutic modality for cancer treatment is radiotherapy, which is currently used for more than 50% of cancer treatments.

Commentato [F3]: As you will see, I stopped revising this section as I think it should be deleted. Actually, all the studies described here are on radiotherapy only: I checked the literature and I found no studies combining RT and HT in the bioceramic field. This option is proposed in the Conclusions as a future possibility.

Radiotherapy mainly uses high-energy radiation like X-rays and **gamma**-rays to kill cancer cells and prevent their proliferation, thus shrinking tumors. In the radiotherapic direct method, radiation starts to disrupt and break the DNA of cancer cells, resulting in cell death by stopping the proliferation procedure. The indirect approach involves the interaction between water molecules and the ionizing radiation, which also leads to DNA damage [164].

One of the most accurate and useful technologies which radiotherapy treatment often relies on is nanotechnology. Among the different types of nanomaterials, gold NPs (AuNPs), silver NPs (AgNPs), silicon NPs (SiNPs), and carbon-based nanomaterials like carbon nanotubes (CNT) are typically used in cancer treatment via radiotherapy (RT) for enhancing radiosensitization [132–135].

Commentato [F4]: These references should be moved to the part on magnetic BGs for HT and discussed there properly.

Various metallic nanomaterials are used in radiotherapy treatments to release localized X-rays or **g**-rays by particle-induced X-ray emission (PIXE) effect and particle-induced **g**-ray emission (PIGE) effect, respectively. AuNPs are a metallic nanostructure with high biocompatible materials with high deposition ability in the tumor volume. Regarding that the solid tumor has a great surrounded blood vessel network, many nanoparticles accumulate around cancer, leading to the enhanced permeability and retention (EPR) effect. According to the high aspect ratio, atomic number, and small volume, AuNPs demonstrate promising candidates for EPR-mediated tumor delivery [135, 136]. Also, it should be mentioned that AuNPs with the atomic number of 79 have a high photoelectric effect since it is positively correlated to $(Z/E)^3$, where E is the incident X-ray energy and Z is the atomic number of the matter. Ma and coworker investigated the effect of a different form of the gold nanostructure comprising gold nanoparticles (GNPs), gold nano spikes (GNSs), and gold nanorods (GNRs). They showed that the GNP revealed the most KB cancer cellular responses and cellular uptake compared to other gold nanostructure types. The radiation sensitizing effect of the gold nanostructures was determined by the amount of Au nanostructure. The sensitization enhancement ratios (SER) of treating three types of the Au nanostructures, including GNPs, GNSS, and GNR, were 1.62, 1.37, and 1.21, respectively. Besides, the higher anticancer efficiency can be obtained corresponding to the treatments of GNPs by X-ray irradiation than other types of Au nanostructures [169].

Commentato [F5]: This part focuses on METALLIC nanomaterials - it is out of scope

Apart from metallic nanomaterials used in this treatment approach, it is also revealed that samarium (Sm) sealed in carbon nanocapsule (single and multiple wall nanotubes) is used for radiotherapy, which exhibits a promising candidate for this treatment method. In this paper, the carbon nanocapsule is first enriched with the ^{152}Sm, then ^{153}Sm is formed by neutron irradiation. As a result, a radioactivity up to 11.37 GBq/mg is observed via neutron irradiation. The prepared

materials are useful both for in vivo imaging and radiotherapeutic [134, 138]. Figure 7 reveals that the single intravenous administration of 20 MBq of the mentioned materials greatly delayed lung tumor growth. The bioluminescence imaging capability of the untreated and treated with the prepared materials on 10 and 16 days after tumor inoculation are demonstrated in Figure 8a. Figure 8b illustrated the average lung weight measurements depicted on day 16 post-tumor inoculation. The average tumor size (photon/s) of different samples displayed that the responses began after 13 days of the tumor inoculation (Figure 8c).

Regarding the similar injection dose and amount of radioactivity, significant tumor growth suppression on day 16 (***$p < 0.001$, compared to control) is observed for both 153Sm@CNT treatments. However, the 153Sm@CNT prevented tumor proliferation, it cannot eradicate the tumors completely. Histological analyses are shown in Figure 8d on hematoxylin and eosin (H&E) and Neutral Red stained lung tissue sections after 16 days of the tumor inoculation. They demonstrated that compared to the untreated mice, 153Sm@CNT treated samples, lung sections are healthier with the presence of fewer colonies of melanoma nodules.

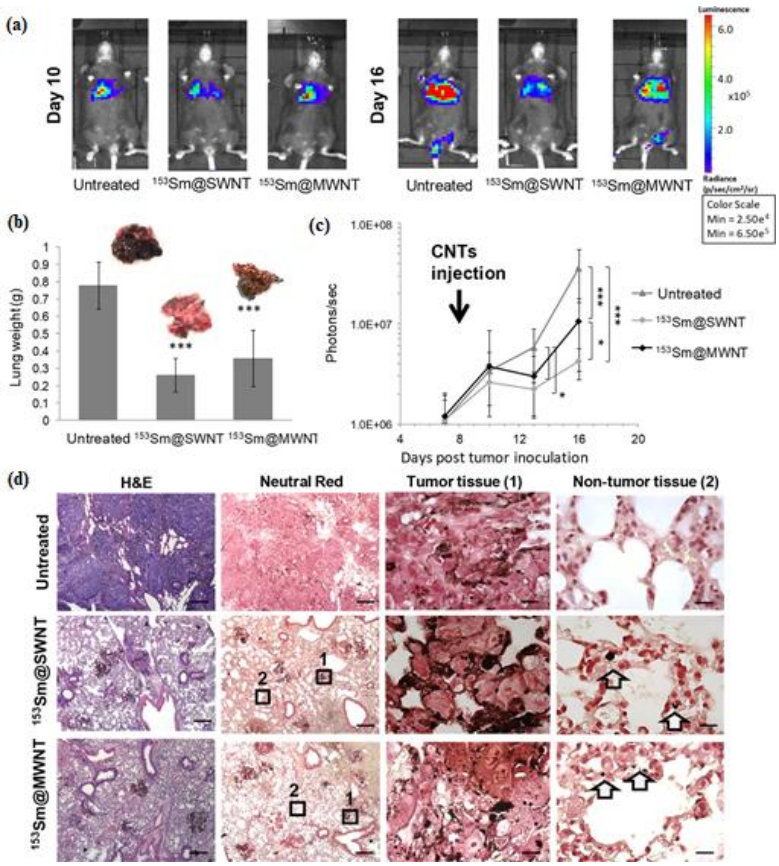

Figure 8- Tumor growth delay studies in experimental metastatic lung tumor mice model after internal administration of radiotherapy. B16F10-Luc tumor-bearing C57BL/6 mice received a single i.v. injection of ^{153}Sm@SWNT or ^{153}Sm@MWNT (20 MBq, 200 μg) on day 8 post-tumor inoculation. (a) Representative whole-body images of untreated, ^{153}Sm@SWNT, and ^{153}Sm@MWNT treated mice captured on days 10 and 16 post-tumor inoculation. (b) Average lung weights measured on day 16 post-tumor inoculation, the experimental endpoint. Tumor growth monitoring over time. Bioluminescence signals correspond to luciferase-expressing B16F10 cells in the lung. (d) H&E and Neutral Red stained B16F10-Luc tumor-containing lung tissue sections excised on day 16 (left panels). High-magnification images of the tumor (areas 1) and nontumor (areas 2) lung tissues are shown on the right. Arrows indicate the presence of CNTs. Scale bars: 200 μm for H&E (histological examination) and Neutral Red (track CNTs) stained sections; 5 μm for zoom-in images of areas 1 and 2. Results are presented as mean ± SD (n = 9−10). Significant differences were examined using one-way ANOVA followed by Tukey's multiple comparison test (*p < 0.05, **p < 0.01, ***p < 0.001).

In another research done by Ruan et al., GQDs exhibited a potential candidate to be used as a nano-radiosensitizer in radiotherapy for cancer treatment. In other words, not only GQDs enhanced the colorectal carcinoma cells' selectivity and sensitivity towards ionizing irradiation, but they also can reduce cell proliferation and enhance apoptosis. The mitochondria get damaged as soon as the GQDs in the presence of irradiation cause increasing ROS [171]. Regarding the combination of radiotherapy with HT, Sadeghi et al. developed temperature-sensitive liposomes (TLS) loaded with the radiosensitizer pimonidazole (PMZ). At high temperature (>42 ^{o}C), the prepared materials start releasing the radiosensitizer in 30 seconds, leading to the breakage of double strands DNA, and PMZ-TSL enhances the radiation efficacy with HT by increasing the cell mortality [172]. In another work, the gadolinium-doped iron oxide nanoparticles (GdIONP) was demonstrated a higher SAR rather than IONPs. This research also revealed the HT effect of GdIONP with or without radiotherapy was investigated. This method was improved the radiation therapy efficiency by reducing the fraction of hypoxic cells. Besides, thermotherapy and radiotherapy's combination leads to the longest tumor growth delay of about 10 days than thermotherapy, and radiotherapy approach alone with 4.5 days and 2.5 days, respectively [173].
Yttrium-doped glasses based on SiO_2–P_2O_5–Na_2O–CaO–Y_2O_3 systems are also used as radioisotope vectors for *in situ* radiotherapy (brachytherapy): for this purpose, glasses do not need to be bioactive, but they must be biocompatible and radioactive to kill malignant tumors [165–167].. Sene et al. illustrated that glass microspheres possess a stable surface to cause cell proliferation and prevent tissue damage in radiotherapy for cancer treatment [174]. In the other work, yttrium (Y)-doped bioactive glass is clinically used as an excellent candidate for selective internal radiotherapy of liver cancer. The active bio-glass helped 90Y isotope in improving the biocompatibility and biodegradability in the body for a long time after treatment. As a result, Y-doped bioactive glass powders were an ideal candidate for radioactive treatment and prevented Y from leaching before radioactive decay [175]. Tilocca et al. revealed that Y doped bioactive glass exchange their ion with the protein in the contact medium and depleted of Na and Ca ions after their exchange, which is partly due to the high bio-glass stability [176]. Regarding the Y doped bioactive glass radiotherapy application, the formation of the stable and durable bio-glass as a contact medium was mainly due to the high glass matrix connectivity by ion exchange. Bi-doped bioglasses can also reduce the residual cancer cells with the help of toxic chemotherapies and

radiation therapies [154]. The authors believe that if HT and radiotherapy are activated simultaneously in BGs, cancer therapy's potency will increase dramatically. It is possible to design a glass composition that has these two capabilities at the same time. More R&D on this subject is highly demanding.

7-2- HT combined with phototherapy

There are two main categories of phototherapeutic approaches for cancer treatment, including photothermal therapy (PTT) and photodynamic therapy (PDT), which have drawn enormous worldwide attention due to the negligible side effects and low systemic toxicity. These approaches are non-invasive photo-triggered tumor treatment. Several research works have been done on the combination of phototherapy and other cancer treatment procedure, which may have the potential to significantly improve cancer therapy efficiency [48]. Although most works focus on the use of metallic NPs, some studies on bioceramics have been reported too. For example, Paula et al. showed that the combination of HT treatment and PDT mediated by maghemite-based NPs could be highly effective for brain cancer inhibition. The results shown in Figure 9a demonstrated a 10% reduction in cell viability without considering MNPs into the nanoemulsion (MNE). Besides, Figure 9b demonstrated the effect of using MNE/ClAlPc formulation and applying HT treatment (~15% reduction of cancer cell viability). The results showed an insignificant change in the cell viability depending on the concentration of MNPs. However, higher cell mortality of about 52 % was detected when the researchers used PDT in the presence of MNE formulation (Figure 9c). The most significant cytotoxic effect to cancer cells (70 %) was observed in Figure 9d when the HT and PDT were used simultaneously, which is higher than ~50% and 10% mortality for the PDT and HT, individually [179].

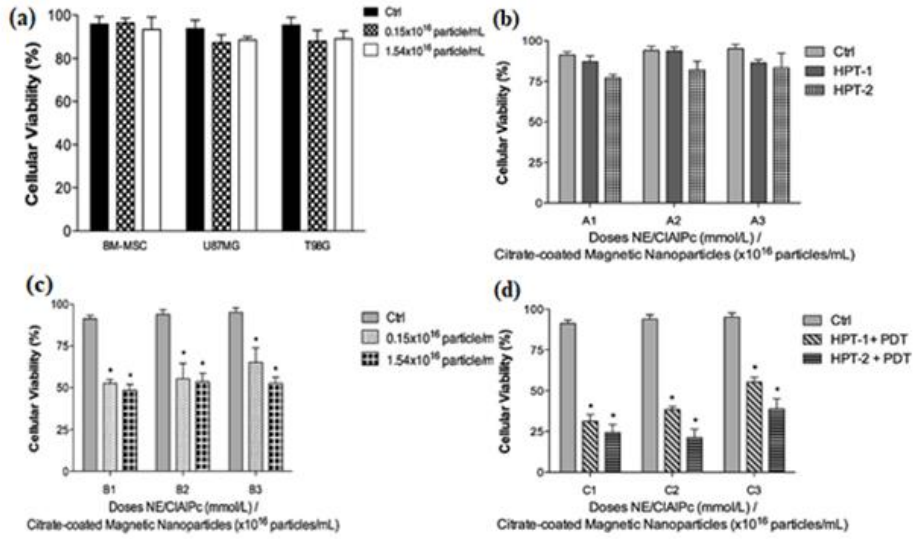

Figure 9 a- Viability of the cell lines incubated with the as-produced MNE/ClAlPc in the absence of HT and PDT. Ctrl – control (cells in medium at 3% serum). There was no statistical difference in the experiment. All data were expressed as the mean SEM of three independent experiments, b- Viability of cell lines incubated at 3 hours with different MNE containing equal contents of encapsulated ClAlPc (0.5 mg mL^{-1}). Ctrl: control (cells in 3% serum medium); A1: BM-MSc; A2: U87MG and A3: T98G; HPT: hyperthermia treatment; HPT-1: 1 MHz/40 Oe + sample containing 0.15 10^{16} magnetic nanoparticle per mL; HPT-2: 1 MHz/40 Oe + sample containing 1.54 10^{16} magnetic nanoparticle per mL. (c) B1: BM-MSc; B2: U87MG and B3: T98G; only evaluation of photodynamic therapy (700 mJ cm^{-2}). d- C1: BM-MSc; C2: U87MG and C3: T98G; PDT: photodynamic therapy (700 mJ cm^{-2}); HPT-1 +PDT: sample containing 0.15 10^{16} magnetic nanoparticle per mL + 700 mJ cm^{-2}; HPT-2 + PDT: sample containing 1.54 10^{16} magnetic nanoparticle per mL + 700 mJ cm^{-2}. Statistical analysis was performed by one-way analysis of variance (ANOVA) and Tukey test. All data were expressed as the mean SEM of three independent experiments. Statistical significance for this study was considered at $*p < 0.05$.

In another work, iron oxide nanoflowers/CuS hybrids were proved to be useful for three therapeutic modalities (HT, PTT and PDT) for cancer treatment [180].

After being properly doped, MBGs have also shown great photothermal activities but, at present, they have not been used for simultaneous HT therapy yet. However, photothermal properties of

MBGs have been combined with other extra-functionalities. Wang et al. synthesized bismuth-doped MBGs that could kill cancer cells via PTT and promote bone regeneration in rats [154].
Furthermore, multi-color fluorescent MBG nanoparticles were developed with high fluorescence intensity so that they can potentially as a multifunctional system for anticancer drug delivery, bioimaging, and phototherapy (PTT, PDT) [182]. NIR light-triggered intelligent manganese (Mn)-doped MBGs loaded with chlorin e6 (Mn-MBG/Ce6) were also used for bone defect therapy. The presence of Mn in the nano-platform promoted the PT effect and yielded a high specific surface area in the material. After Ce6 loading, the Mn-doped MBG displayed controlled Ce6 release by NIR light, which improved the PDT efficiency.
It is worth pointing out that PTT modality is a more efficient approach than the magnetic HT method for cancer therapy. However, regarding the location of the tumor inside the body, magnetic HT could be preferred. In deeply entangled tumors in which laser cannot penetrate, magnetic HT should be employed, but in other tumors that are not deep in the body, PTT can easily be applied. Besides, if magnetic NPs are injected into the tumour site for HT treatment, the tumor location can be observed by magnetic resonance imaging (MRI) due to the presence of the magnetic core in the nanostructure.

8- Conclusion and perspective

The major input that one can have after looking at the existing literature on magnetic HT for cancer treatment is that a truly strong collaboration between materials scientists, biologists and clinicians will truly be key to further progress in this field. In fact, in spite of the high number of publications on *in vitro* and *in vivo* (animal studies) aspects of magnetic HT, there are still many gaps to bridge for establishing a clear correlation between these results and what actually happens in the clinical scenario.
At present, superparamagnetic iron oxide NPs are marketed for clinical use [ref], but their use in cancer therapy has some shortcomings. An old, well-known problem of NPs is how to control that all of them actually reaches the tumor, avoiding that a fraction of the injected NPs may be allocated outside the cancer site in other organs [ref]. Another issue related to the clinical use of

NPs is that they may undergo phagocytosis by the host immune system, thus being unable to reaching the target site with an obvious decrease of the magnetic HT therapy efficacy [ref]. If the tumor site is difficult to reach by NPs, such approach is unfeasible and/or ineffective. Furthermore, even if the external magnetic field can guide the NPs through the bloodstream to the cancer site, during this "travel" the NPs can be surface coated or somehow bound by the body biomolecules, which can thus prevent them from reaching the target area [ref].

All these "clinical" and "biological" problems potentially happen for all the bioceramic NPs used for magnetic HT, including iron oxide systems, ferrites, BGs and BGCs etc.

Another crucial issue related to bioceramic for magnetic HT concerns the only partial understanding of the relationships that exist between magnetic properties and physico-chemical characteristics, such as particle size and shape, microstructure, crystalline phase and role of dopants. Furthermore, some ideal characteristics of the materials still need to be fixed, such as ideal particle size and shape. Likewise, the preferable administration route (e.g. subcutaneous, intraperitoneal, intramuscular or intravenous injection) still is an open issue – and, in this regard, the opinion of clinicians would play a key role. Finally, the parameters of the "best" applied field are another critical concern, as well as the "best" non-invasive method for performing an accurate temperature control. The latter aspect is essential because HT-induced overheating can damage the normal tissue that surrounds the tumor [ref].

Magnetic NPs for HT applications have been traditionally made of insoluble materials in order to avoid the leaching of potentially toxic ions in the body. In this way, however, they are totally unable to stimulate tissue regeneration. This is a very critical aspect deserving careful attention. When bone cancer is surgically removed, a large void is typically created which can involve weakening of surrounding bone. Furthermore, even after tumor removal, some malignant cells may survive around the tumor site, leading to tumor recurrence. In order to overcome this couple of problems, the use of magnetic BGs and BGCs can be a valuable option: once implanted, these materials may stimulate healthy bone regeneration and undergo reheating process - when necessary - to kill residual or newly-formed cancerous cells. Additionally, BGs can be produced in a number of forms besides micro- and nanoparticles – e.g. 3D porous scaffolds, injectable pastes etc. – which can match the defect dimensions and further contribute to the healing process [ref]. On the other, it cannot be ignored that BGs can also stimulate angiogenesis [ref], which is

strongly involved in cancer growth: therefore, if implantation of magnetic BGs/BGCs can be a good option after benign tumor curettage, the same option could not be so advisable in the case of malignancy. Hence, implantation of BGs/BGCs at bone tumors sites must be carefully considered and discussed with oncologists, and relevant studies deserve to be performed in the future.

One of the main challenges related to developing multifunctional BGs and BGCs for magnetic HT concerns the combination of bioactive and magnetic properties. The presence of magnetic phases in the glass matrix decreases the bioactivity and iron can be easily segregated, forming non-magnetic crystals (e.g. hematite) during thermal treatment. On the other hand, incorporation of low amounts of iron in the glass can be a limiting factor from a magnetic viewpoint, leading to insufficient amount of magnetic phase to generate the heat required for HT treatment [ref]. BGs also carry the potential of being used for imparting additional extra-functionalities, such as drug release and photothermal therapy. Thus, great promise comes from systems eliciting multiple therapeutic actions against cancer, in which HT is synergistically combined with chemotherapy and photothermal therapy. An interesting field for future research, which has not been apparently investigated so far, could deal with the development of BGs and BGCs with magnetic and radioactive properties, thus combining HT therapy and radiotherapy.

Finally, surface functionalization and coating strategies [ref] applied to magnetic BGs and bioceramics are versatile and novel approaches to improve biocompatibility (especially in non-bioactive crystalline ceramics) and imparting additional anticancer functions (e.g. drug delivery mediated by stimuli-responsive hydrogel coatings).

Commentato [F6]: Singh, R.K., Kothiyal, G.P., Srinivasan, A.: Magnetic and structural properties of CaO–SiO2–P2O5–Na2O–Fe2O3 glass ceramics. J. Magn. Magn. Mater. 320, 1352–1356 (2008)

Commentato [F7]: S. Kargozar, F. Kermani, S.M. Beidokhti, S. Hamzehlou, E. Verné, S. Ferraris, F. Baino. Functionalization and surface modifications of bioactive glasses (BGs): tailoring of the biological response working on the outermost surface layer. Materials 2019;12:3696

Reference

[1] K. Mahmoudi, A. Bouras, D. Bozec, R. Ivkov, and C. Hadjipanayis, “Magnetic hyperthermia therapy for the treatment of glioblastoma: a review of the therapy’s history, efficacy and application in humans,” *Int. J. Hyperth.*, vol. 34, no. 8, pp. 1316–1328, 2018.

[2] S. Kargozar, M. Mozafari, S. Hamzehlou, H.-W. Kim, and F. Baino, “Mesoporous bioactive glasses (MBGs) in cancer therapy: Full of hope and promise,” *Mater. Lett.*, vol. 251, pp. 241–246, 2019.

[3] M. Montazerian, E. D. Zanotto, and J. C. Mauro, “Model-driven design of bioactive glasses: from molecular dynamics through machine learning,” *Int. Mater. Rev.*, vol. 65, no. 5, pp. 297–321, 2020.

[4] K. Maier-Hauff *et al.*, “Intracranial thermotherapy using magnetic nanoparticles combined with external beam radiotherapy: results of a feasibility study on patients with glioblastoma multiforme,” *J. Neurooncol.*, vol. 81, no. 1, pp. 53–60, 2007.

[5] > Peter Wust *et al.*, “Magnetic nanoparticles for interstitial thermotherapy–feasibility, tolerance and achieved temperatures,” *Int. J. Hyperth.*, vol. 22, no. 8, pp. 673–685, 2006.

[6] A. Matsumine *et al.*, “Novel hyperthermia for metastatic bone tumors with magnetic

materials by generating an alternating electromagnetic field," *Clin. Exp. Metastasis*, vol. 24, no. 3, pp. 191–200, 2007.

[7] M. Johannsen *et al.*, "Morbidity and quality of life during thermotherapy using magnetic nanoparticles in locally recurrent prostate cancer: results of a prospective phase I trial," *Int. J. Hyperth.*, vol. 23, no. 3, pp. 315–323, 2007.

[8] M. Johannsen, B. Thiesen, P. Wust, and A. Jordan, "Magnetic nanoparticle hyperthermia for prostate cancer," *Int. J. Hyperth.*, vol. 26, no. 8, pp. 790–795, 2010.

[9] F. Benyettou *et al.*, "Covalent Organic Framework Embedded with Magnetic Nanoparticles for MRI and Chemo-Thermotherapy," *J. Am. Chem. Soc.*, vol. 142, no. 44, pp. 18782–18794, 2020.

[10] A. Amani, J. M. Begdelo, H. Yaghoubi, and S. Motallebinia, "Multifunctional magnetic nanoparticles for controlled release of anticancer drug, breast cancer cell targeting, MRI/fluorescence imaging, and anticancer drug delivery," *J. Drug Deliv. Sci. Technol.*, vol. 49, pp. 534–546, 2019.

[11] H. Xie, J. Dong, J. Duan, J. Hou, S. Ai, and X. Li, "Magnetic nanoparticles-based immunoassay for aflatoxin B1 using porous g-C3N4 nanosheets as fluorescence probes," *Sensors Actuators B Chem.*, vol. 278, pp. 147–152, 2019.

[12] P. Das, M. Colombo, and D. Prosperi, "Recent advances in magnetic fluid hyperthermia for cancer therapy," *Colloids Surfaces B Biointerfaces*, vol. 174, pp. 42–55, 2019.

[13] E. Umut, M. Coşkun, F. Pineider, D. Berti, and H. Güngüneş, "Nickel ferrite nanoparticles for simultaneous use in magnetic resonance imaging and magnetic fluid hyperthermia," *J. Colloid Interface Sci.*, vol. 550, pp. 199–209, 2019.

[14] D. Bahadur and J. Giri, "Biomaterials and magnetism," *Sadhana*, vol. 28, no. 3–4, pp. 639–656, 2003.

[15] P. C. Naha *et al.*, "Dextran-coated iron oxide nanoparticles as biomimetic catalysts for localized and pH-activated biofilm disruption," *ACS Nano*, vol. 13, no. 5, pp. 4960–4971, 2019.

[16] T. Javanbakht, S. Laurent, D. Stanicki, and E. David, "Related physicochemical, rheological, and dielectric properties of nanocomposites of superparamagnetic iron oxide nanoparticles with polyethyleneglycol," *J. Appl. Polym. Sci.*, vol. 137, no. 3, p. 48280, 2020.

[17] T. N. Le, T. D. Tran, and M. Il Kim, "A Convenient Colorimetric Bacteria Detection Method Utilizing Chitosan-Coated Magnetic Nanoparticles," *Nanomaterials*, vol. 10, no. 1, p. 92, 2020.

[18] H. Zhao, C. Zhang, D. Qi, T. Lü, and D. Zhang, "One-Step synthesis of polyethylenimine-coated magnetic nanoparticles and its demulsification performance in surfactant-stabilized oil-in-water emulsion," *J. Dispers. Sci. Technol.*, vol. 40, no. 2, pp. 231–238, 2019.

[19] A. Alaghmandfard and H. R. Madaah Hosseini, "A facile, two-step synthesis and

characterization of Fe3O4–LCysteine–graphene quantum dots as a multifunctional nanocomposite," *Appl. Nanosci.*, 2021, doi: 10.1007/s13204-020-01642-1.

[20] V. V Mody, A. Singh, and B. Wesley, "Basics of magnetic nanoparticles for their application in the field of magnetic fluid hyperthermia," *Eur. J. Nanomedicine*, vol. 5, no. 1, pp. 11–21, 2013.

[21] J. S. Lee, J. M. Cha, H. Y. Yoon, J.-K. Lee, and Y. K. Kim, "Magnetic multi-granule nanoclusters: A model system that exhibits universal size effect of magnetic coercivity," *Sci. Rep.*, vol. 5, no. 1, pp. 1–7, 2015.

[22] P. Weerathunge *et al.*, "Transferrin-conjugated quasi-cubic SPIONs for cellular receptor profiling and detection of brain cancer," *Sensors Actuators B Chem.*, vol. 297, p. 126737, 2019.

[23] Z. Xu *et al.*, "Seed-mediated growth of ultra-thin triangular magnetite nanoplates," *Chem. Commun.*, vol. 53, no. 80, pp. 11052–11055, 2017.

[24] D. W. Wong, W. L. Gan, Y. K. Teo, and W. S. Lew, "Heating Efficiency of Triple Vortex State Cylindrical Magnetic Nanoparticles," *Nanoscale Res. Lett.*, vol. 14, no. 1, p. 376, 2019.

[25] P. Bury *et al.*, "Effect of spherical magnetic particles on liquid crystals behavior studied by surface acoustic waves," *J. Magn. Magn. Mater.*, vol. 423, pp. 57–60, 2017.

[26] A. Lu, E. emsp14L Salabas, and F. Schüth, "Magnetic nanoparticles: synthesis, protection, functionalization, and application," *Angew. Chemie Int. Ed.*, vol. 46, no. 8, pp. 1222–1244, 2007.

[27] P. Yuan, D. Li, L. Wu, and L. Shi, "Synthesis and growth mechanism of monodispersed BiFeO3 nanorods with controllable aspect ratio and magnetic/optical properties," *Ceram. Int.*, vol. 46, no. 1, pp. 1243–1247, 2020.

[28] Y. Chao *et al.*, "Iron nanoparticles for low-power local magnetic hyperthermia in combination with immune checkpoint blockade for systemic antitumor therapy," *Nano Lett.*, vol. 19, no. 7, pp. 4287–4296, 2019.

[29] Y. Du, X. Liu, Q. Liang, X.-J. Liang, and J. Tian, "Optimization and design of magnetic ferrite nanoparticles with uniform tumor distribution for highly sensitive MRI/MPI performance and improved magnetic hyperthermia therapy," *Nano Lett.*, vol. 19, no. 6, pp. 3618–3626, 2019.

[30] Z. Hedayatnasab, F. Abnisa, and W. M. A. W. Daud, "Review on magnetic nanoparticles for magnetic nanofluid hyperthermia application," *Mater. Des.*, vol. 123, pp. 174–196, 2017.

[31] X. Yao *et al.*, "Graphene quantum dots-capped magnetic mesoporous silica nanoparticles as a multifunctional platform for controlled drug delivery, magnetic hyperthermia, and photothermal therapy," *Small*, vol. 13, no. 2, p. 1602225, 2017.

[32] X. Wang *et al.*, "Near-Infrared Triggered Release of uPA from Nanospheres for Localized

Hyperthermia-Enhanced Thrombolysis," *Adv. Funct. Mater.*, vol. 27, no. 40, p. 1701824, 2017.

[33] S. Ghosh, K. Ghosal, S. A. Mohammad, and K. Sarkar, "Dendrimer functionalized carbon quantum dot for selective detection of breast cancer and gene therapy," *Chem. Eng. J.*, vol. 373, pp. 468–484, 2019.

[34] M. J. Podolska *et al.*, "Graphene Oxide Nanosheets for Localized Hyperthermia—Physicochemical Characterization, Biocompatibility, and Induction of Tumor Cell Death," *Cells*, vol. 9, no. 3, p. 776, 2020.

[35] B. Kozissnik, A. C. Bohorquez, J. Dobson, and C. Rinaldi, "Magnetic fluid hyperthermia: advances, challenges, and opportunity," *Int. J. Hyperth.*, vol. 29, no. 8, pp. 706–714, 2013.

[36] D. Chang *et al.*, "Biologically targeted magnetic hyperthermia: potential and limitations," *Front. Pharmacol.*, vol. 9, p. 831, 2018.

[37] R. D. Aspasio, R. Borges, and J. Marchi, "Biocompatible glasses for cancer treatment," in *Biocompatible Glasses*, Springer, 2016, pp. 249–265.

[38] R. Karimian and B. Goldoost, "Review the effect of hyperthermia using iron and magnetic nanoparticles in cancer treatment in chemical injuries," *J. Adv. Pharm. Educ. Res. Apr-Jun*, vol. 9, no. S2, 2019.

[39] A. Yadollahpour and S. A. Hosseini, "Magnetic nanoparticle based hyperthermia: A review of the physiochemical properties and synthesis methods," *Int J Pharm Res Allied Sci*, vol. 5, pp. 242–246, 2016.

[40] R. K. Gilchrist, W. D. Shorey, R. C. Hanselman, F. A. DePeyster, J. Yang, and R. Medal, "Effects of electromagnetic heating on internal viscera a preliminary to the treatment of human tumors," *Ann. Surg.*, vol. 161, no. 6, p. 890, 1965.

[41] A. G. Kolhatkar, A. C. Jamison, D. Litvinov, R. C. Willson, and T. R. Lee, "Tuning the magnetic properties of nanoparticles," *Int. J. Mol. Sci.*, vol. 14, no. 8, pp. 15977–16009, 2013.

[42] R.-J. Chung, H.-Y. Wang, and K.-T. Wu, "Preparation and characterization of Fe-Au alloy nanoparticles for hyperthermia application," *J. Med. Biol. Eng*, vol. 34, no. 3, p. 251, 2014.

[43] K. L. McNerny, Y. Kim, D. E. Laughlin, and M. E. McHenry, "Chemical synthesis of monodisperse γ-Fe–Ni magnetic nanoparticles with tunable Curie temperatures for self-regulated hyperthermia," *J. Appl. Phys.*, vol. 107, no. 9, p. 09A312, 2010.

[44] A. Salati, A. Ramazani, and M. A. Kashi, "Tuning hyperthermia properties of FeNiCo ternary alloy nanoparticles by morphological and magnetic characteristics," *J. Magn. Magn. Mater.*, vol. 498, p. 166172, 2020.

[45] C. C. Berry and A. S. G. Curtis, "Functionalisation of magnetic nanoparticles for applications in biomedicine," *J. Phys. D. Appl. Phys.*, vol. 36, no. 13, p. R198, 2003.

[46] M. Safi, J. Courtois, M. Seigneuret, H. Conjeaud, and J.-F. Berret, “The effects of aggregation and protein corona on the cellular internalization of iron oxide nanoparticles,” *Biomaterials*, vol. 32, no. 35, pp. 9353–9363, 2011, doi: https://doi.org/10.1016/j.biomaterials.2011.08.048.

[47] R. Hergt, S. Dutz, R. Müller, and M. Zeisberger, “Magnetic particle hyperthermia: nanoparticle magnetism and materials development for cancer therapy,” *J. Phys. Condens. Matter*, vol. 18, no. 38, p. S2919, 2006.

[48] A. Alaghmandfard *et al.*, “Recent advances in the modification of carbon-based quantum dots for biomedical applications,” *Mater. Sci. Eng. C*, p. 111756, 2020.

[49] K. Zhang, G. Li, Z. Pei, S. Zhao, A. Jing, and G. Liang, “Injectable graphite-modified Fe3O4/calcium phosphate bone cement with enhanced heating ability for hyperthermia,” *Mater. Technol.*, vol. 35, no. 13–14, pp. 863–871, 2020, doi: 10.1080/10667857.2019.1706809.

[50] C. Xu *et al.*, “Magnetic Hyperthermia Ablation of Tumors Using Injectable Fe3O4/Calcium Phosphate Cement,” *ACS Appl. Mater. Interfaces*, vol. 7, no. 25, pp. 13866–13875, Jul. 2015, doi: 10.1021/acsami.5b02077.

[51] M. V Velasco, M. T. Souza, M. C. Crovace, A. J. A. de Oliveira, and E. D. Zanotto, “Bioactive magnetic glass-ceramics for cancer treatment,” *Biomed. Glas.*, vol. 5, no. 1, pp. 148–177, 2019.

[52] Y. Ebisawa, T. Kokubo, K. Ohura, and T. Yamamuro, “Bioactivity of Fe 2 O 3-containing CaO-SiO 2 glasses: in vitro evaluation,” *J. Mater. Sci. Mater. Med.*, vol. 4, no. 3, pp. 225–232, 1993.

[53] 川下将一, 岩橋康臣, 小久保正, 八尾健, 濱田直, and 新庄輝也, “Preparation of glass-ceramics containing ferrimagnetic zinc-iron ferrite for the hyperthermal treatment of cancer,” *J. Ceram. Soc. Japan*, vol. 112, no. 1307, pp. 373–379, 2004.

[54] P. Intawin, W. Leenakul, P. Jantaratana, A. Munpakdee, and K. Pengpat, “Fabrication of SrFe12O19-P2O5-CaO-Na2O Bioactive Glass-Ceramics at Various Sintering Temperatures,” *Ferroelectrics*, vol. 489, no. 1, pp. 35–42, 2015.

[55] P. Intawin, W. Leenakul, P. Jantaratana, and K. Pengpat, “Fabrication and magnetic properties of P2O5-CaO-Na2O bioactive glass ceramic containing BaFe12O19,” *Integr. Ferroelectr.*, vol. 148, no. 1, pp. 171–177, 2013.

[56] G. Li, S. Feng, and D. Zhou, “Magnetic bioactive glass ceramic in the system CaO–P 2 O 5–SiO 2–MgO–CaF 2–MnO 2–Fe 2 O 3 for hyperthermia treatment of bone tumor,” *J. Mater. Sci. Mater. Med.*, vol. 22, no. 10, p. 2197, 2011.

[57] V. Daboin *et al.*, “Magnetic SiO2-Mn1-xCoxFe2O4 nanocomposites decorated with Au@ Fe3O4 nanoparticles for hyperthermia,” *J. Magn. Magn. Mater.*, vol. 479, pp. 91–98, 2019.

[58] J. Suárez, V. Daboin, G. González, and S. Briceño, “Chitosan-polyvinylpyrrolidone

CoxFe3− xO4 (0.25≤ x≤ 1) nanoparticles for hyperthermia applications," *Int. J. Biol. Macromol.*, vol. 164, pp. 3403–3410, 2020.

[59] P. B. Balakrishnan *et al.*, "Exploiting Unique Alignment of Cobalt Ferrite Nanoparticles, Mild Hyperthermia, and Controlled Intrinsic Cobalt Toxicity for Cancer Therapy," *Adv. Mater.*, vol. 32, no. 45, p. 2003712, 2020.

[60] L. H. Nguyen *et al.*, "Increase of magnetic hyperthermia efficiency due to optimal size of particles: theoretical and experimental results," *J. Nanoparticle Res.*, vol. 22, no. 9, pp. 1–16, 2020.

[61] I. Castellanos-Rubio *et al.*, "Outstanding heat loss via nano-octahedra above 20 nm in size: from wustite-rich nanoparticles to magnetite single-crystals," *Nanoscale*, vol. 11, no. 35, pp. 16635–16649, 2019.

[62] D. Liang *et al.*, "Coprecipitation synthesis of N, Fe doped anatase TiO 2 nanoparticles and photocatalytic mechanism," *J. Mater. Sci. Mater. Electron.*, vol. 30, no. 13, pp. 12619–12629, 2019.

[63] I. Nkurikiyimfura, Y. Wang, B. Safari, and E. Nshingabigwi, "Temperature-dependent magnetic properties of magnetite nanoparticles synthesized via coprecipitation method," *J. Alloys Compd.*, vol. 846, p. 156344, 2020.

[64] L. Gutiérrez *et al.*, "Aggregation effects on the magnetic properties of iron oxide colloids," *Nanotechnology*, vol. 30, no. 11, p. 112001, 2019.

[65] S. P. Yeap, J. Lim, B. S. Ooi, and A. L. Ahmad, "Agglomeration, colloidal stability, and magnetic separation of magnetic nanoparticles: collective influences on environmental engineering applications," *J. Nanoparticle Res.*, vol. 19, no. 11, p. 368, 2017.

[66] H. Qi, Z. Li, H. Zheng, L. Fu, and Q. Jia, "Facile preparation of hydrophilic glutathione modified magnetic nanomaterials for specific enrichment of glycopeptides," *Chinese Chem. Lett.*, vol. 30, no. 12, pp. 2181–2185, 2019.

[67] X. Deng, W. Li, G. Ding, T. Xue, and X. Chen, "Synthesis and applications of functionalized magnetic nanomaterials in enantioseparation," *Sep. Purif. Rev.*, vol. 48, no. 1, pp. 14–29, 2019.

[68] V. Iannotti *et al.*, "Fe-doping-induced magnetism in nano-hydroxyapatites," *Inorg. Chem.*, vol. 56, no. 8, pp. 4446–4458, 2017.

[69] A. D. Sharma and H. B. Sharma, "Electrical and magnetic properties of Mn-doped BiFeO3 nanomaterials," *Integr. Ferroelectr.*, vol. 203, no. 1, pp. 81–90, 2019.

[70] N. Zhao *et al.*, "Synthesis, Structure, and Magnetic Properties of B-Doped Fe3N@ C Magnetic Nanomaterial as Catalyst for the Hydrogen Evolution Reaction," *Phys. status solidi*, vol. 256, no. 12, p. 1900111, 2019.

[71] Â. L. Andrade *et al.*, "An efficient and simple procedure to prepare chemically stable and partially carbon-cleaned magnetite from solid-state synthesis for clinical practices in medical oncology," *Mater. Today Commun.*, vol. 25, p. 101612, 2020.

[72] A. Villanueva *et al.*, "Hyperthermia HeLa cell treatment with silica-coated manganese oxide nanoparticles," *J. Phys. Chem. C*, vol. 114, no. 5, pp. 1976–1981, 2010.

[73] R. A. Youness, M. A. Taha, H. Elhaes, and M. Ibrahim, "Molecular modeling, FTIR spectral characterization and mechanical properties of carbonated-hydroxyapatite prepared by mechanochemical synthesis," *Mater. Chem. Phys.*, vol. 190, pp. 209–218, 2017.

[74] V. Narayanaswamy *et al.*, "Synthesis of graphene oxide-Fe3O4 based nanocomposites using the mechanochemical method and in vitro magnetic hyperthermia," *Int. J. Mol. Sci.*, vol. 20, no. 13, p. 3368, 2019.

[75] R. Ahmadi and H. R. M. Hosseini, "An investigation on the optimum conditions of synthesizing a magnetite based ferrofluid as MRI contrast agent using Taguchi method," *Mater. Sci. Pol.*, vol. 31, no. 2, pp. 253–258, 2013, doi: 10.2478/s13536-012-0098-9.

[76] R. Ahmadi *et al.*, "Ultrasonic-assisted synthesis of magnetite based MRI contrast agent using cysteine as the biocapping coating," *Mater. Chem. Phys.*, vol. 131, no. 1–2, pp. 170–177, 2011, doi: 10.1016/j.matchemphys.2011.04.083.

[77] S. Gyergyek *et al.*, "Hydrothermal growth of iron oxide NPs with a uniform size distribution for magnetically induced hyperthermia: Structural, colloidal and magnetic properties," *J. Alloys Compd.*, vol. 694, pp. 261–271, 2017.

[78] S. Fayazzadeh, M. Khodaei, M. Arani, S. R. Mahdavi, T. Nizamov, and A. Majouga, "Magnetic Properties and Magnetic Hyperthermia of Cobalt Ferrite Nanoparticles Synthesized by Hydrothermal Method," *J. Supercond. Nov. Magn.*, pp. 1–7, 2020.

[79] F. Baino *et al.*, "Fe-doped sol-gel glasses and glass-ceramics for magnetic hyperthermia," *Materials (Basel).*, vol. 11, no. 1, p. 173, 2018.

[80] A. Farzin, R. Emadi, and M. Fathi, "Novel sol–gel-derived hardystonite-based biomagnetic nanoparticles for hyperthermia applications," *J. Sol-Gel Sci. Technol.*, vol. 80, no. 2, pp. 402–410, 2016.

[81] B. Pimentel *et al.*, "Threshold heating temperature for magnetic hyperthermia: controlling the heat exchange with the blocking temperature of magnetic nanoparticles," *J. Solid State Chem.*, vol. 260, pp. 34–38, 2018.

[82] A. Sathya, S. Kalyani, S. Ranoo, and J. Philip, "One-step microwave-assisted synthesis of water-dispersible Fe3O4 magnetic nanoclusters for hyperthermia applications," *J. Magn. Magn. Mater.*, vol. 439, pp. 107–113, 2017.

[83] H. Hu *et al.*, "Unique role of ionic liquid in microwave-assisted synthesis of monodisperse magnetite nanoparticles," *Chem. Commun.*, vol. 46, no. 22, pp. 3866–3868, 2010.

[84] Y.-J. Liang *et al.*, "Size-dependent electromagnetic properties and the related simulations of Fe3O4 nanoparticles made by microwave-assisted thermal decomposition," *Colloids Surfaces A Physicochem. Eng. Asp.*, vol. 530, pp. 191–199, 2017.

[85] M. H. Ehsani, S. Esmaeili, M. Aghazadeh, P. Kameli, and I. Karimzadeh, "Magnetic evaluation of the nanoparticles coated with polyvinylpyrrolidone and polyvinyl chloride

nanoparticles synthesized by electro-deposition method for hyperthermia application," *J. Supercond. Nov. Magn.*, vol. 32, no. 7, pp. 2021–2030, 2019.

[86] J. A. Fuentes-García, A. Carvalho Alavarse, A. C. Moreno Maldonado, A. Toro-Córdova, M. R. Ibarra, and G. F. Goya, "Simple Sonochemical Method to Optimize the Heating Efficiency of Magnetic Nanoparticles for Magnetic Fluid Hyperthermia," *ACS omega*, vol. 5, no. 41, pp. 26357–26364, 2020.

[87] K. Kombaiah, J. J. Vijaya, L. J. Kennedy, M. Bououdina, and B. Al-Najar, "Conventional and microwave combustion synthesis of optomagnetic CuFe2O4 nanoparticles for hyperthermia studies," *J. Phys. Chem. Solids*, vol. 115, pp. 162–171, 2018.

[88] A. Gaona-Esquivel, D. S. Hernández-Manzo, P. J. Sánchez-Trujillo, O. E. Cigarroa-Mayorga, and M. Meléndez-Lira, "Hyperthermia Effect on Phantom of Breast Carcinoma Tissue Induced by Mn3O4 Nanoparticles Synthesized by One-Step Spray Pyrolysis Method," in *Key Engineering Materials*, 2020, vol. 853, pp. 56–60.

[89] F. Baino, G. Novajra, and C. Vitale-Brovarone, "Bioceramics and scaffolds: a winning combination for tissue engineering," *Front. Bioeng. Biotechnol.*, vol. 3, p. 202, 2015.

[90] J. R. Woodard *et al.*, "The mechanical properties and osteoconductivity of hydroxyapatite bone scaffolds with multi-scale porosity," *Biomaterials*, vol. 28, no. 1, pp. 45–54, 2007.

[91] J. Park, S. Bauer, K. von der Mark, and P. Schmuki, "Nanosize and vitality: TiO2 nanotube diameter directs cell fate," *Nano Lett.*, vol. 7, no. 6, pp. 1686–1691, 2007.

[92] M. Scheffler and P. Colombo, *Cellular ceramics: structure, manufacturing, properties and applications*. John Wiley & Sons, 2006.

[93] H. Sun *et al.*, "3D printing of calcium phosphate scaffolds with controlled release of antibacterial functions for jaw bone repair," *Mater. Des.*, vol. 189, p. 108540, 2020.

[94] B. Zhang *et al.*, "Porous bioceramics produced by inkjet 3D printing: effect of printing ink formulation on the ceramic macro and micro porous architectures control," *Compos. Part B Eng.*, vol. 155, pp. 112–121, 2018.

[95] B. Zhang *et al.*, "The biomimetic design and 3D printing of customized mechanical properties porous Ti6Al4V scaffold for load-bearing bone reconstruction," *Mater. Des.*, vol. 152, pp. 30–39, 2018.

[96] C. Gosselin, R. Duballet, P. Roux, N. Gaudillière, J. Dirrenberger, and P. Morel, "Large-scale 3D printing of ultra-high performance concrete–a new processing route for architects and builders," *Mater. Des.*, vol. 100, pp. 102–109, 2016.

[97] S. Fu, X. Du, M. Zhu, Z. Tian, D. Wei, and Y. Zhu, "3D printing of layered mesoporous bioactive glass/sodium alginate-sodium alginate scaffolds with controllable dual-drug release behaviors," *Biomed. Mater.*, vol. 14, no. 6, p. 65011, 2019.

[98] F. Baino *et al.*, "Processing methods for making porous bioactive glass-based scaffolds—A state-of-the-art review," *Int. J. Appl. Ceram. Technol.*, vol. 16, no. 5, pp. 1762–1796, 2019.

[99] H. Ma, C. Feng, J. Chang, and C. Wu, “3D-printed bioceramic scaffolds: From bone tissue engineering to tumor therapy,” *Acta Biomater.*, vol. 79, pp. 37–59, 2018.

[100] I. K. Januariyasa and Y. Yusuf, “Porous carbonated hydroxyapatite-based scaffold using simple gas foaming method,” *J. Asian Ceram. Soc.*, no. just-accepted, 2020.

[101] M. Navarro *et al.*, “New macroporous calcium phosphate glass ceramic for guided bone regeneration,” *Biomaterials*, vol. 25, no. 18, pp. 4233–4241, 2004, doi: https://doi.org/10.1016/j.biomaterials.2003.11.012.

[102] A. Almirall, G. Larrecq, J. A. Delgado, S. Martınez, J. A. Planell, and M. P. Ginebra, “Fabrication of low temperature macroporous hydroxyapatite scaffolds by foaming and hydrolysis of an α-TCP paste,” *Biomaterials*, vol. 25, no. 17, pp. 3671–3680, 2004.

[103] Z. Huan, J. Chang, and J. Zhou, “Low-temperature fabrication of macroporous scaffolds through foaming and hydration of tricalcium silicate paste and their bioactivity,” *J. Mater. Sci.*, vol. 45, no. 4, pp. 961–968, 2010.

[104] P. Sepulveda, J. R. Jones, and L. L. Hench, “Bioactive sol-gel foams for tissue repair,” *J. Biomed. Mater. Res. An Off. J. Soc. Biomater. Japanese Soc. Biomater. Aust. Soc. Biomater. Korean Soc. Biomater.*, vol. 59, no. 2, pp. 340–348, 2002.

[105] X. Zhang *et al.*, “Template-assisted, sol-gel fabrication of biocompatible, hierarchically porous hydroxyapatite scaffolds,” *Materials (Basel).*, vol. 12, no. 8, p. 1274, 2019.

[106] J. Zhang, J. Zhou, X. Huang, L. Wang, G. Liu, and J. Cheng, “In situ preparation of hierarchically porous β-tricalcium phosphate bioceramic scaffolds by the sol-gel method combined with F127,” *Ceram. Int.*, vol. 46, no. 5, pp. 6396–6405, 2020.

[107] L. de Siqueira, R. F. Gouveia, L. Grenho, F. J. Monteiro, M. H. Fernandes, and E. S. Trichês, “Highly porous 45S5 bioglass-derived glass–ceramic scaffolds by gelcasting of foams,” *J. Mater. Sci.*, vol. 53, no. 15, pp. 10718–10731, 2018.

[108] L. Siqueira *et al.*, “Preparation, Characterization and Biological Studies of B-TCP and B-TCP/Al2O3 Scaffolds Obtained by Gel-Casting of Foams,” *Mater. Res.*, vol. 20, no. 4, pp. 973–983, 2017.

[109] F. Baino, E. Verné, and C. Vitale-Brovarone, “3-D high-strength glass–ceramic scaffolds containing fluoroapatite for load-bearing bone portions replacement,” *Mater. Sci. Eng. C*, vol. 29, no. 6, pp. 2055–2062, 2009, doi: https://doi.org/10.1016/j.msec.2009.04.002.

[110] F. Darus, R. M. Isa, N. Mamat, and M. Jaafar, “Techniques for fabrication and construction of three-dimensional bioceramic scaffolds: Effect on pores size, porosity and compressive strength,” *Ceram. Int.*, vol. 44, no. 15, pp. 18400–18407, 2018.

[111] I. Denry and L. T. Kuhn, “Design and characterization of calcium phosphate ceramic scaffolds for bone tissue engineering,” *Dent. Mater.*, vol. 32, no. 1, pp. 43–53, 2016.

[112] A. Kordjamshidi, S. Saber-Samandari, M. G. Nejad, and A. Khandan, “Preparation of novel porous calcium silicate scaffold loaded by celecoxib drug using freeze drying technique: Fabrication, characterization and simulation,” *Ceram. Int.*, vol. 45, no. 11, pp.

14126–14135, 2019.

[113] X. Du, S. Fu, and Y. Zhu, “3D printing of ceramic-based scaffolds for bone tissue engineering: an overview,” *J. Mater. Chem. B*, vol. 6, no. 27, pp. 4397–4412, 2018.

[114] T. Ruthradevi *et al.*, “Investigations on nickel ferrite embedded calcium phosphate nanoparticles for biomedical applications,” *J. Alloys Compd.*, vol. 695, pp. 3211–3219, 2017.

[115] B. Srinivasan *et al.*, “Thermally Modified Iron-Inserted Calcium Phosphate for Magnetic Hyperthermia in an Acceptable Alternating Magnetic Field,” *J. Phys. Chem. B*, vol. 123, no. 26, pp. 5506–5513, 2019.

[116] A. Adamiano *et al.*, “Magnetic calcium phosphates nanocomposites for the intracellular hyperthermia of cancers of bone and brain,” *Nanomedicine*, vol. 14, no. 10, pp. 1267–1289, 2019.

[117] C.-H. Hou, S.-M. Hou, Y.-S. Hsueh, J. Lin, H.-C. Wu, and F.-H. Lin, “The in vivo performance of biomagnetic hydroxyapatite nanoparticles in cancer hyperthermia therapy,” *Biomaterials*, vol. 30, no. 23, pp. 3956–3960, 2009, doi: https://doi.org/10.1016/j.biomaterials.2009.04.020.

[118] J. A. Ramos-Guivar, M. A. Morales, and F. J. Litterst, “γ-Fe2O3 nanoparticles embedded in nanohydroxyapatite matrix for magnetic hyperthermia and in vitro osteoblast cell studies,” *Ceram. Int.*, 2020.

[119] M. Mozafari, M. Rabiee, M. Azami, and S. Maleknia, “Biomimetic formation of apatite on the surface of porous gelatin/bioactive glass nanocomposite scaffolds,” *Appl. Surf. Sci.*, vol. 257, no. 5, pp. 1740–1749, 2010.

[120] S. Kargozar, M. Montazerian, S. Hamzehlou, H.-W. Kim, and F. Baino, “Mesoporous bioactive glasses: Promising platforms for antibacterial strategies,” *Acta Biomater.*, vol. 81, pp. 1–19, 2018.

[121] H. Jain *et al.*, *Bioactive glasses: Fundamentals, technology and applications*. Royal Society of Chemistry, 2016.

[122] M. Montazerian and E. Dutra Zanotto, “History and trends of bioactive glass-ceramics,” *J. Biomed. Mater. Res. Part A*, vol. 104, no. 5, pp. 1231–1249, 2016.

[123] Y. Ebisawa, F. Miyaji, T. Kokubo, K. Ohura, and T. Nakamura, “Bioactivity of ferrimagnetic glass-ceramics in the system FeO□ Fe2O3□ CaO□ SiO2,” *Biomaterials*, vol. 18, no. 19, pp. 1277–1284, 1997.

[124] X. Qi *et al.*, “Three dimensional printing of calcium sulfate and mesoporous bioactive glass scaffolds for improving bone regeneration in vitro and in vivo,” *Sci. Rep.*, vol. 7, no. 1, p. 42556, 2017, doi: 10.1038/srep42556.

[125] A. A. Luderer *et al.*, “Glass-ceramic-mediated, magnetic-field-induced localized hyperthermia: response of a murine mammary carcinoma,” *Radiat. Res.*, vol. 94, no. 1, pp. 190–198, 1983.

[126] S. Oh, S. Choi, Y. Lee, and K. Kim, “Research on annihilation of cancer cells by glass-ceramics for cancer treatment with external magnetic field. I. Preparation and cytotoxicity,” *J. Biomed. Mater. Res. An Off. J. Soc. Biomater. Japanese Soc. Biomater.*, vol. 54, no. 3, pp. 360–365, 2001.

[127] P. Ji, Y. Wang, M. Zhang, B. Li, and G. Zhang, “P2O5-Fe2O3-CaO-SiO2 ferromagnetic glass-ceramics for hyperthermia,” *Int. J. Appl. Ceram. Technol.*, vol. 15, no. 5, pp. 1261–1267, 2018.

[128] G. F. Baronzio and E. D. Hager, *Hyperthermia in cancer treatment: a primer*. Springer Science & Business Media, 2008.

[129] G. Li *et al.*, “Study on the interface between bioactive glass and magnetite,” *Compos. Interfaces*, vol. 27, no. 7, pp. 687–703, 2020, doi: 10.1080/09276440.2019.1688046.

[130] R. Koohkan, T. Hooshmand, D. Mohebbi-Kalhori, M. Tahriri, and M. T. Marefati, “Synthesis, characterization, and in vitro biological evaluation of copper-containing magnetic bioactive glasses for hyperthermia in bone defect treatment,” *ACS Biomater. Sci. Eng.*, vol. 4, no. 5, pp. 1797–1811, 2018.

[131] T. Wang *et al.*, “The development of magnetic degradable DP-Bioglass for hyperthermia cancer therapy,” *J. Biomed. Mater. Res. Part A An Off. J. Soc. Biomater. Japanese Soc. Biomater. Aust. Soc. Biomater. Korean Soc. Biomater.*, vol. 83, no. 3, pp. 828–837, 2007.

[132] G. Da Li, Y. Lin, T. H. Pan, G. S. Chen, and Q. D. Yin, “Synthesis and characterization of magnetic bioactive glass-ceramics containing Mg ferrite for hyperthermia,” *Mater. Sci. Eng. C*, vol. 30, no. 1, pp. 148–153, 2010.

[133] W. Leenakul, P. Kantha, N. Pisitpipathsin, G. Rujijanagul, S. Eitssayeam, and K. Pengpat, “Structural and magnetic properties of SiO2–CaO–Na2O–P2O5 containing BaO–Fe2O3 glass–ceramics,” *J. Magn. Magn. Mater.*, vol. 325, pp. 102–106, 2013.

[134] W. Leenakul, J. Ruangsuriya, P. Jantaratana, and K. Pengpat, “Fabrication and characterization of ferrimagnetic bioactive glass-ceramic containing BaFe12O19,” *Ceram. Int.*, vol. 39, pp. S201–S205, 2013.

[135] W. Leenakul, P. Intawin, J. Ruangsuriya, P. Jantaratana, and K. Pengpat, “Magnetic bioactive SrFe12O19-SiO2-CaO-Na2O-P2O5 glass-ceramics for hyperthermia treatment of bone cancer,” *Integr. Ferroelectr.*, vol. 148, no. 1, pp. 81–89, 2013.

[136] Y. Ebisawa, Y. SUGIMOTO, T. HAYASHI, T. KOKUBO, K. OHURA, and T. YAMAMURO, “Crystallization of (FeO, Fe2O3)-CaO-SiO2 glasses and magnetic properties of their crystallized products,” *J. Ceram. Soc. Japan*, vol. 99, no. 1145, pp. 7–13, 1991.

[137] K. Ohura *et al.*, “A heat-generating bioactive glass–ceramic for hyperthermia,” *J. Appl. Biomater.*, vol. 2, no. 3, pp. 153–159, 1991.

[138] O. Bretcanu, S. Spriano, E. Verne, M. Cöisson, P. Tiberto, and P. Allia, “The influence of crystallised Fe3O4 on the magnetic properties of coprecipitation-derived ferrimagnetic

glass–ceramics," *Acta Biomater.*, vol. 1, no. 4, pp. 421–429, 2005.

[139] R. K. Singh and A. Srinivasan, "Apatite-forming ability and magnetic properties of glass-ceramics containing zinc ferrite and calcium sodium phosphate phases," *Mater. Sci. Eng. C*, vol. 30, no. 8, pp. 1100–1106, 2010.

[140] R. K. Singh and A. Srinivasan, "Magnetic properties of bioactive glass-ceramics containing nanocrystalline zinc ferrite," *J. Magn. Magn. Mater.*, vol. 323, no. 3–4, pp. 330–333, 2011.

[141] S. A. Shah, M. U. Hashmi, S. Alam, and A. Shamim, "Magnetic and bioactivity evaluation of ferrimagnetic ZnFe2O4 containing glass ceramics for the hyperthermia treatment of cancer," *J. Magn. Magn. Mater.*, vol. 322, no. 3, pp. 375–381, 2010.

[142] C.-S. Hsi, H.-Z. Cheng, H.-J. Hsu, Y.-S. Chen, and M.-C. Wang, "Crystallization kinetics and magnetic properties of iron oxide contained 25Li2O–8MnO2–20CaO–2P2O5–45SiO2 glasses," *J. Eur. Ceram. Soc.*, vol. 27, no. 10, pp. 3171–3176, 2007.

[143] D. Arcos, R. P. Del Real, and M. Vallet-Regı, "A novel bioactive and magnetic biphasic material," *Biomaterials*, vol. 23, no. 10, pp. 2151–2158, 2002.

[144] D. Arcos, R. P. Del Real, and M. Vallet-Regí, "Biphasic materials for bone grafting and hyperthermia treatment of cancer," *J. Biomed. Mater. Res. Part A An Off. J. Soc. Biomater. Japanese Soc. Biomater. Aust. Soc. Biomater. Korean Soc. Biomater.*, vol. 65, no. 1, pp. 71–78, 2003.

[145] M. C. Serrano *et al.*, "In vitro positive biocompatibility evaluation of glass–glass ceramic thermoseeds for hyperthermic treatment of bone tumors," *Tissue Eng. Part A*, vol. 14, no. 5, pp. 617–627, 2008.

[146] A. Yazdanpanah, F. Moztarzadeh, and S. Arabyazdi, "A heat-generating lithium-ferrite doped bioactive glass for cancer hyperthermia," *Phys. B Condens. Matter*, p. 412298, 2020.

[147] G. Li *et al.*, "A novel method to enhance magnetic property of bioactive glass-ceramics for hyperthermia," *Ceram. Int.*, vol. 45, no. 4, pp. 4945–4956, 2019.

[148] Y. Y. Wang, B. Li, W. Q. Luo, and F. Cao, "Bioactivity of Fe2O3-CaO-SiO2 glass ceramics modified through the addition of P2O5 and TiO2," *Ceram. Int.*, vol. 43, no. 9, pp. 6738–6745, 2017.

[149] E. Fiume, C. Migneco, E. Verné, and F. Baino, "Comparison between Bioactive Sol-Gel and Melt-Derived Glasses/Glass-Ceramics Based on the Multicomponent SiO2–P2O5–CaO–MgO–Na2O–K2O System," *Materials (Basel).*, vol. 13, no. 3, p. 540, 2020.

[150] X. Kesse *et al.*, "Elaboration of Superparamagnetic and Bioactive Multicore–Shell Nanoparticles (γ-Fe2O3@SiO2-CaO): A Promising Material for Bone Cancer Treatment," *ACS Appl. Mater. Interfaces*, vol. 12, no. 42, pp. 47820–47830, Oct. 2020, doi: 10.1021/acsami.0c12769.

[151] R. Borges, L. Mendonça-Ferreira, C. Rettori, I. S. O. Pereira, F. Baino, and J. Marchi,

"New sol-gel-derived magnetic bioactive glass-ceramics containing superparamagnetic hematite nanocrystals for hyperthermia application," *Mater. Sci. Eng. C*, p. 111692, 2020.

[152] M. Tripathy, S. Padhiari, and G. Hota, "l-Cysteine-Functionalized Mesoporous Magnetite Nanospheres: Synthesis and Adsorptive Application toward Arsenic Remediation," *J. Chem. Eng. Data*, vol. 65, no. 8, pp. 3906–3919, 2020.

[153] R. K. Singh and A. Srinivasan, "Bioactivity of ferrimagnetic MgO–CaO–SiO2–P2O5–Fe2O3 glass-ceramics," *Ceram. Int.*, vol. 36, no. 1, pp. 283–290, 2010.

[154] L. Wang *et al.*, "Multi-functional bismuth-doped bioglasses: combining bioactivity and photothermal response for bone tumor treatment and tissue repair," *Light Sci. Appl.*, vol. 7, no. 1, p. 1, 2018, doi: 10.1038/s41377-018-0007-z.

[155] Z. Tian, X. Yu, Z. Ruan, M. Zhu, Y. Zhu, and N. Hanagata, "Magnetic mesoporous silica nanoparticles coated with thermo-responsive copolymer for potential chemo- and magnetic hyperthermia therapy," *Microporous Mesoporous Mater.*, vol. 256, pp. 1–9, 2018, doi: https://doi.org/10.1016/j.micromeso.2017.07.053.

[156] H. Keshavarz, A. Khavandi, S. Alamolhoda, and M. R. Naimi-Jamal, "Magnetite mesoporous silica nanoparticles embedded in carboxybetaine methacrylate for application in hyperthermia and drug delivery," *New J. Chem.*, vol. 44, no. 20, pp. 8232–8240, 2020, doi: 10.1039/D0NJ00939C.

[157] E. Guisasola, L. Asín, L. Beola, J. M. de la Fuente, A. Baeza, and M. Vallet-Regí, "Beyond Traditional Hyperthermia: In Vivo Cancer Treatment with Magnetic-Responsive Mesoporous Silica Nanocarriers," *ACS Appl. Mater. Interfaces*, vol. 10, no. 15, pp. 12518–12525, Apr. 2018, doi: 10.1021/acsami.8b02398.

[158] M. Shoaib, M. S. ur Rahman, A. Saeed, and M. M. Naseer, "Mesoporous bioactive glass-polyurethane nanocomposites as reservoirs for sustained drug delivery," *Colloids Surfaces B Biointerfaces*, vol. 172, pp. 806–811, 2018.

[159] A. Seyfoori, S. A. S. Ebrahimi, S. Omidian, and S. M. Naghib, "Multifunctional magnetic ZnFe2O4-hydroxyapatite nanocomposite particles for local anti-cancer drug delivery and bacterial infection inhibition: an in vitro study," *J. Taiwan Inst. Chem. Eng.*, vol. 96, pp. 503–508, 2019.

[160] W. Luo, B. Li, Y. Wang, G. Pan, and H. Wu, "Synthesis of multifunctional hollow SiO2-CaO-Fe2O3 glass-ceramic nanospheres," *Int. J. Appl. Ceram. Technol.*, vol. 17, no. 4, pp. 1843–1851, 2020.

[161] H. Zhang, W. Zhang, Y. Zhou, Y. Jiang, and S. Li, "Dual functional mesoporous silicon nanoparticles enhance the radiosensitivity of VPA in glioblastoma," *Transl. Oncol.*, vol. 10, no. 2, pp. 229–240, 2017.

[162] Z. Liu *et al.*, "Enhancement of radiotherapy efficacy by silver nanoparticles in hypoxic glioma cells," *Artif. cells, nanomedicine, Biotechnol.*, vol. 46, no. sup3, pp. S922–S930, 2018.

[163] J. T.-W. Wang *et al.*, “Neutron-irradiated antibody-functionalised carbon nanocapsules for targeted cancer radiotherapy,” *Carbon N. Y.*, 2020.

[164] N. Goswami, Z. Luo, X. Yuan, D. T. Leong, and J. Xie, “Engineering gold-based radiosensitizers for cancer radiotherapy,” *Mater. Horizons*, vol. 4, no. 5, pp. 817–831, 2017.

[165] S. Kargozar, M. Montazerian, E. Fiume, and F. Baino, “Multiple and promising applications of Sr-containing bioactive glasses in bone tissue engineering,” *Front. Bioeng. Biotechnol.*, vol. 7, p. 161, 2019.

[166] Y. Lin, J. C. Mauro, and G. Kaur, “Bioactive glasses for cancer therapy,” in *Biomedical, therapeutic and clinical applications of bioactive glasses*, Elsevier, 2019, pp. 273–312.

[167] D. E. Day, “Glasses for radiotherapy,” *Bio-Glasses; John Wiley Sons, Ltd. Hoboken, NJ, USA*, pp. 203–228, 2012.

[168] G. Song, L. Cheng, Y. Chao, K. Yang, and Z. Liu, “Emerging nanotechnology and advanced materials for cancer radiation therapy,” *Adv. Mater.*, vol. 29, no. 32, p. 1700996, 2017.

[169] N. Ma *et al.*, “Shape-dependent radiosensitization effect of gold nanostructures in cancer radiotherapy: comparison of gold nanoparticles, nanospikes, and nanorods,” *ACS Appl. Mater. Interfaces*, vol. 9, no. 15, pp. 13037–13048, 2017.

[170] J. T.-W. Wang *et al.*, “Neutron activated 153Sm sealed in carbon nanocapsules for in vivo imaging and tumor radiotherapy,” *ACS Nano*, vol. 14, no. 1, pp. 129–141, 2019.

[171] J. Ruan *et al.*, “Graphene quantum dots for radiotherapy,” *ACS Appl. Mater. Interfaces*, vol. 10, no. 17, pp. 14342–14355, 2018.

[172] N. Sadeghi *et al.*, “Hyperthermia-triggered release of hypoxic cell radiosensitizers from temperature-sensitive liposomes improves radiotherapy efficacy in vitro,” *Nanotechnology*, vol. 30, no. 26, p. 264001, 2019.

[173] P.-S. Jiang, H.-Y. Tsai, P. Drake, F.-N. Wang, and C.-S. Chiang, “Gadolinium-doped iron oxide nanoparticles induced magnetic field hyperthermia combined with radiotherapy increases tumour response by vascular disruption and improved oxygenation,” *Int. J. Hyperth.*, vol. 33, no. 7, pp. 770–778, 2017.

[174] F. F. Sene, J. R. Martinelli, and E. Okuno, “Synthesis and characterization of phosphate glass microspheres for radiotherapy applications,” *J. Non. Cryst. Solids*, vol. 354, no. 42–44, pp. 4887–4893, 2008.

[175] A. Hadush Tesfay *et al.*, “Control of dopant distribution in yttrium-doped bioactive glass for selective internal radiotherapy applications using spray pyrolysis,” *Materials (Basel).*, vol. 12, no. 6, p. 986, 2019.

[176] A. Tilocca, “Realistic models of bioactive glass radioisotope vectors in practical conditions: structural effects of ion exchange,” *J. Phys. Chem. C*, vol. 119, no. 49, pp. 27442–27448, 2015.

[177] A. Zhang, W. Guo, Y. Qi, J. Wang, X. Ma, and D. Yu, “Synergistic effects of gold nanocages in hyperthermia and radiotherapy treatment,” *Nanoscale Res. Lett.*, vol. 11, no. 1, pp. 1–14, 2016.

[178] Y. Deng *et al.*, “Dual-light triggered metabolizable nano-micelles for selective tumor-targeted photodynamic/hyperthermia therapy,” *Acta Biomater.*, 2020.

[179] L. B. De Paula, F. L. Primo, M. R. Pinto, P. C. Morais, and A. C. Tedesco, “Evaluation of a chloroaluminium phthalocyanine-loaded magnetic nanoemulsion as a drug delivery device to treat glioblastoma using hyperthermia and photodynamic therapy,” *Rsc Adv.*, vol. 7, no. 15, pp. 9115–9122, 2017.

[180] A. Curcio *et al.*, “Iron oxide nanoflowers@ CuS hybrids for cancer tri-therapy: Interplay of photothermal therapy, magnetic hyperthermia and photodynamic therapy,” *Theranostics*, vol. 9, no. 5, p. 1288, 2019.

[181] L. Ma *et al.*, “Multifunctional bioactive Nd-Ca-Si glasses for fluorescence thermometry, photothermal therapy, and burn tissue repair,” *Sci. Adv.*, vol. 6, no. 32, p. eabb1311, 2020.

[182] R. K. Singh *et al.*, “Label-Free Fluorescent Mesoporous Bioglass for Drug Delivery, Optical Triple-Mode Imaging, and Photothermal/Photodynamic Synergistic Cancer Therapy,” *ACS Appl. Bio Mater.*, vol. 3, no. 4, pp. 2218–2229, 2020.